Present-day kinematics and fault slip rates in eastern Iran, derived from 11 years of GPS data

A. Walpersdorf, I. Manighetti, Z. Mousavi, F. Tavakoli, M. Vergnolle, A. Jadidi, D. Hatzfeld, A. Aghamohammadi, A. Bigot, Y. Djamour, et al.

AGU PUBLICATIONS

JGR

Journal of Geophysical Research: Solid Earth

RESEARCH ARTICLE
10.1002/2013JB010620

Key Points:
- New, dense GPS data constrains present-day kinematics in central eastern Iran
- Current slip rates measured on most active faults in central eastern Iran
- Convergence mainly accommodated through vertical axis block rotations

Supporting Information:
- Readme
- Figure S1
- Figure S2
- Figure S3
- Figure S4
- Figure S5

Correspondence to:
A. Walpersdorf,
andrea.walpersdorf@ujf-grenoble.fr

Citation:
Walpersdorf, A., et al. (2014), Present-day kinematics and fault slip rates in eastern Iran, derived from 11 years of GPS data, *J. Geophys. Res. Solid Earth*, *119*, 1359–1383, doi:10.1002/2013JB010620.

Received 20 AUG 2013
Accepted 3 JAN 2014
Accepted article online 8 JAN 2014
Published online 18 FEB 2014

Present-day kinematics and fault slip rates in eastern Iran, derived from 11 years of GPS data

A. Walpersdorf[1], I. Manighetti[2], Z. Mousavi[1,3], F. Tavakoli[3], M. Vergnolle[2], A. Jadidi[3], D. Hatzfeld[1], A. Aghamohammadi[3], A. Bigot[2], Y. Djamour[3], H. Nankali[3], and M. Sedighi[3]

[1]ISTerre, CNRS UMR 5275, Université Joseph Fourier, Grenoble, France, [2]GeoAZUR, Université de Nice Sophia-Antipolis, CNRS, IRD, Observatoire de la Côte d'Azur, Sophia Antipolis, France, [3]Geodetic Department, National Cartographic Center, Tehran, Iran

Abstract We analyze new GPS data spanning 11 years at 92 stations in eastern Iran. We use these data to analyze the present-day kinematics and the slip rates on most seismogenic faults in eastern Iran. The east Lut, west Lut, Kuhbanan, Anar, Dehshir, and Doruneh faults are confirmed as the major faults and are found to currently slip laterally at 5.6 ± 0.6, 4.4 ± 0.4, 3.6 ± 1.3, 2.0 ± 0.7, 1.4 ± 0.9, and 1.3 ± 0.8 mm/yr, respectively. Slip is right-lateral on the ~NS striking east Lut, west Lut, Kuhbanan, Anar, and Dehshir faults and left-lateral on the ~EW Doruneh fault. The ~NS faults slice the eastern Iranian crust into five blocks that are moving northward at 6–13 mm/yr with respect to the stable Afghan crust at the eastern edge of the collision zone. The collective behavior of the ~NS faults might thus allow the Arabian promontory to impinge northward into the Eurasian crust. The ~NS faults achieve additional NS shortening by rotating counterclockwise in the horizontal plane, at current rates up to 0.8°/Ma. Modeling the GPS and available geological data with a block rotation model suggests that the rotations have been going on at a similar rate (1 ± 0.4°/Ma) over the last 12 Ma. We identify large strains at the tips of the rotating east Lut, west Lut, and Kuhbanan faults, which we suspect to be responsible for the important historical and instrumental seismicity in those zones.

1. Introduction

Iran has been extensively studied over the last decades because its territory offers the rare opportunity to observe and quantify how the convergence between two plates—Arabia and Eurasia—has been accommodated from its onset to its present-day continuation, i.e., continental collision within Iran. Additionally, Iran is the site of frequent devastating earthquakes, and it is thus of critical importance to understand how those earthquakes emerge from the overall tectonics that affects the Iranian territory.

As a result of the many prior investigations that have been conducted in Iran [e.g., *Berberian*, 1976, 1981; *Nowroozi and Mohajer-Ashjai*, 1985; *Bellier et al*., 1997; *Walker and Jackson*, 2004; *Allen et al*., 2004; *Vernant et al*., 2004a; *Masson et al*., 2005; *Reilinger et al*., 2006; *Meyer et al*., 2006; *Hollingsworth et al*., 2010a; *Farbod et al*., 2011; *Cifelli et al*., 2013; *Nozaem et al*., 2013], the general features of the Cenozoic to present-day tectonics in Iran are well recognized. First, the overall kinematics of the Iranian collision zone is broadly understood [e.g., *Jackson et al*., 1995; *Talebian and Jackson*, 2002; *Allen et al*., 2011 and references therein]. The convergence is almost N-S and operates at about 2.5 cm/yr at the longitude of eastern Iran [e.g., *Sella et al*., 2002; *McClusky et al*., 2003; *Vernant et al*., 2004a; *Reilinger et al*., 2006]. To the southeast, the collision zone is bounded by active subduction in the Makran region. To the west, the north and east Anatolian faults form a strike-slip boundary to the collision zone. To the east, the limit of the zone is less clear and is considered to be diffuse and to stop at the political boundary between Iran and Afghanistan/Pakistan. Most of the compression occurs at the southern and northern edges of the collision zone, in the Zagros and in the Alborz and Kopeh Dagh mountains, respectively. In between those thrust and fold belts, a number of strike-slip and reverse faults dissect the Iranian territory. Second, most seismogenic faults have been identified throughout Iran [e.g., *Berberian and Yeats*, 1999; *Walker and Jackson*, 2004; *Walker et al*., 2004, 2009, 2010; *Allen et al*., 2004, 2006, 2011, 2013], and the relationships between those faults and the largest instrumental and historical earthquakes are fairly well understood. Finally, the overall distribution of present-day deformation in Iran begins to be known, thanks to the development of dense GPS networks over the last

decades [e.g., *Nilforoushan et al*., 2003; *Vernant et al*., 2004a, 2004b; *Masson et al*., 2005, 2007; *Walpersdorf et al*., 2006; *Tavakoli*, 2007; *Tavakoli et al*., 2008].

However, a number of key questions remain unanswered, especially in eastern Iran (defined between ~52 and 62°E), which forms the eastern diffuse boundary of the collision zone. Eastern Iran is indeed unique as it is the only part of the territory to show ~N-S to NNW trending faults, almost parallel to the convergence vector. Those faults are long (>100 km), right-lateral, and seismogenic. They are spatially associated with faults having very different orientations and kinematics. Although many tectonic and paleoseismological studies have been conducted on the eastern Iranian faults [e.g., *Allen et al*., 2011 and references therein], it is still unclear how those faults have been and are still currently accommodating the convergence and the related shortening. Different models have been proposed [e.g., *Jackson and McKenzie*, 1984; *Walker and Jackson*, 2004; *Walker and Khatib*, 2006; *Shabanian et al*., 2009b; *Hollingsworth et al*., 2010a; *Allen et al*., 2006, 2011] but data are still lacking to validate them. In particular, despite large efforts, little is known on the current slip rates of the eastern Iranian faults.

Another issue in eastern Iran concerns the understanding of the relationships between "major" and "secondary" faults. Indeed, although eastern Iran is dissected by around ten well-identified, several hundreds of kilometer-long faults that are presumed to accommodate most of the strain and to slip at fast rates (i.e., the so-called "major" faults), there also exist a large number of smaller faults associated with the major structures (i.e., the so-called "secondary" faults). While these secondary faults are likely to accommodate less strain and slip at lower rates than the major faults, a number of them broke in large devastating earthquakes in historical times whereas the major faults were basically quiescent (e.g., earthquakes of Mohammadabad 1941 [*Berberian and Yeats*, 1999; *Walker et al*., 2004], Dustabad 1947 [*Walker et al*., 2004], Ferdows 1968 and Tabas 1978 [*Walker et al*., 2003], South Golbaf [*Berberian and Qorashi*, 1994; *Berberian et al*., 2001], Sefidabeh 1994 [*Berberian et al*., 2000; *Parsons et al*., 2006], Chahar-Farsakh 1998 [*Berberian et al*., 2001], Bam 2003 [e.g., *Talebian et al*., 2004], Dahuyieh (Zarand) 2005 [*Talebian et al*., 2006], and Konarak 2010 [*Foroutan et al*., 2010]; all are highlighted in Figure 1). The peculiar seismic behavior of the secondary faults in eastern Iran thus calls for the need to understand why their slip occurs and how those smaller seismogenic faults might be related to the major ones.

Our objective is to contribute to addressing the above issues. We approach them through a combined tectonic and geodetic (GPS) analysis. We first examine the overall geometry and organization of the active faults in eastern Iran with an emphasis on the relationships between major and secondary faults. We then analyze new, dense GPS data (92 stations) to quantify the current strain and the slip rates on all major and most secondary faults in eastern Iran. The GPS data were acquired over the last 11 years in the framework of the long-going Iranian-French scientific collaboration. Taken together, the tectonic and geodetic data combined with available information, such as long-term fault slip rates, provide constraints on the kinematics of the recent (i.e., last few 10^4–10^6 years) to current deformation in eastern Iran. This understanding in turn provides a guide to better understand the seismic behavior of the secondary faults in eastern Iran.

2. Overall Organization of Active Faults in Eastern Iran

All principal seismogenic faults in eastern Iran are known and their recent to current activity is not in dispute (see references below). A number of fault maps have thus been produced. However, those maps either show most of the faults with simplified traces [e.g., *Walker and Jackson*, 2002; *Walker et al*., 2004; *Meyer and Le Dortz*, 2007; *Le Dortz et al*., 2009; *Allen et al*., 2011; *Farbod et al*., 2011; *Nozaem et al*., 2013] or provide very detailed mapping of isolated faults or local fault sections only [e.g., *Walker and Jackson*, 2002; *Walker et al*., 2004; *Meyer et al*., 2006; *Walker and Khatib*, 2006; *Meyer and Le Dortz*, 2007; *Fattahi et al*., 2007; *Allen et al*., 2011; *Farbod et al*., 2011]. To examine the relationship between major and secondary faults and to properly analyze the GPS data, we need a georeferenced, precise tectonic map that shows all active faults together, major and secondary, in great detail. Therefore, using satellite imagery (panchromatic and color Landsat and Advanced Spaceborn Thermal Emission and Reflection Radiometer (ASTER) images, resolution 15–30 m), topographic data (Shuttle Radar Topography Mission (SRTM) and ASTER digital elevation models, resolution 30–90 m), and information from the literature, we mapped the eastern Iranian faults, at a large (Figure 1) and at a small scale (Figure2). We georeferenced the fault traces with the Ermapper software. It is now well established that most seismogenic faults can be unambiguously recognized from the specific trace that they imprint in the surface

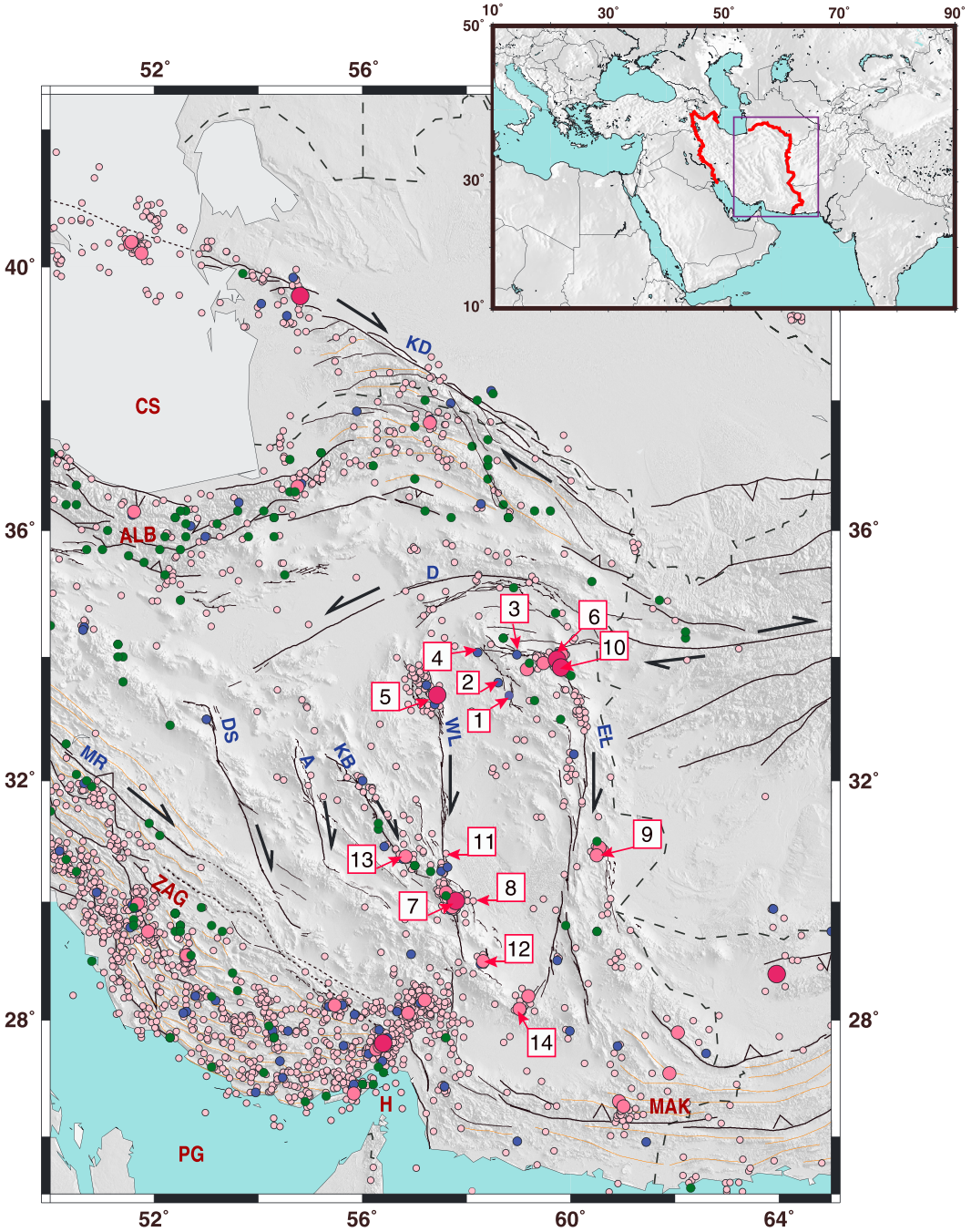

Figure 1. Map of the major active faults in eastern Iran, along with seismicity. Inset presents general location of Iran and of Figure 1. SRTM topography is shown in background. Faults are in black. Thick and thin lines represent respectively major and secondary faults at this scale. Arrows indicate sense of lateral slip while triangles indicate reverse components of slip. Dotted lines are used for faults for which the morphological evidences of recent activity are subtle or possibly disputable. Orange thin lines approximate major fold axes. Dashed lines represent political borders. A: Anar fault; D: Doruneh fault; DS: Dehshir fault; EL: east Lut fault; KB: Kuhbanan fault; KD: Kopeh Dagh fault; MR: Main Recent fault; WL: west Lut fault; ALB: Alborz; CS: Caspian Sea; H: Hormuz straight; MAK: Makran; PG: Persian Gulf; ZAG: Zagros. Green dots present historical earthquakes before 1900 [from *Ambraseys and Melville*, 1982]; blue dots indicate instrumental seismicity from a centennial earthquake catalog [*Engdahl and Villaseñor*, 2002]. Pink dots show instrumental earthquakes from 1973 to 2012 (from USGS catalog NEIC: http://neic.usgs.gov/neis/epic/). Small, medium, and large dots represent magnitudes *Mw* between 4.5 and 6, between 6 and 7, and above 7, respectively. Numbers indicate eastern Iranian earthquakes that are mentioned in text: 1-Mohammadabad 1941; 2-Dustabad 1947 (*Mw* 6.9); 3-Dasht-e-Bayaz 1968 (*Mw* 7.1); 4-Ferdows 1968 (*Mw* 6.2); 5-Tabas 1978 (*Mw* 7.4); 6-Dasht-e-Bayaz 1979 (*Mw* 7.1); 7-Sirch 1981 (*Mw* 7.3); 8-South Golbaf 1989 (*Mw* 5.6); 9-Sefidabeh 1994 (*Mw* 6.1); 10-Zirkuh 1997 (*Mw* 7.2); 11-Chahar-Farsakh 1998 (*Mw* 5.4); 12-Bam 2003 (*Mw* 6.6); 13-Dahuyieh (Zarand) 2005 (*Mw* 6.4); 14-Konarak 2010 (*Mw* 6.7).

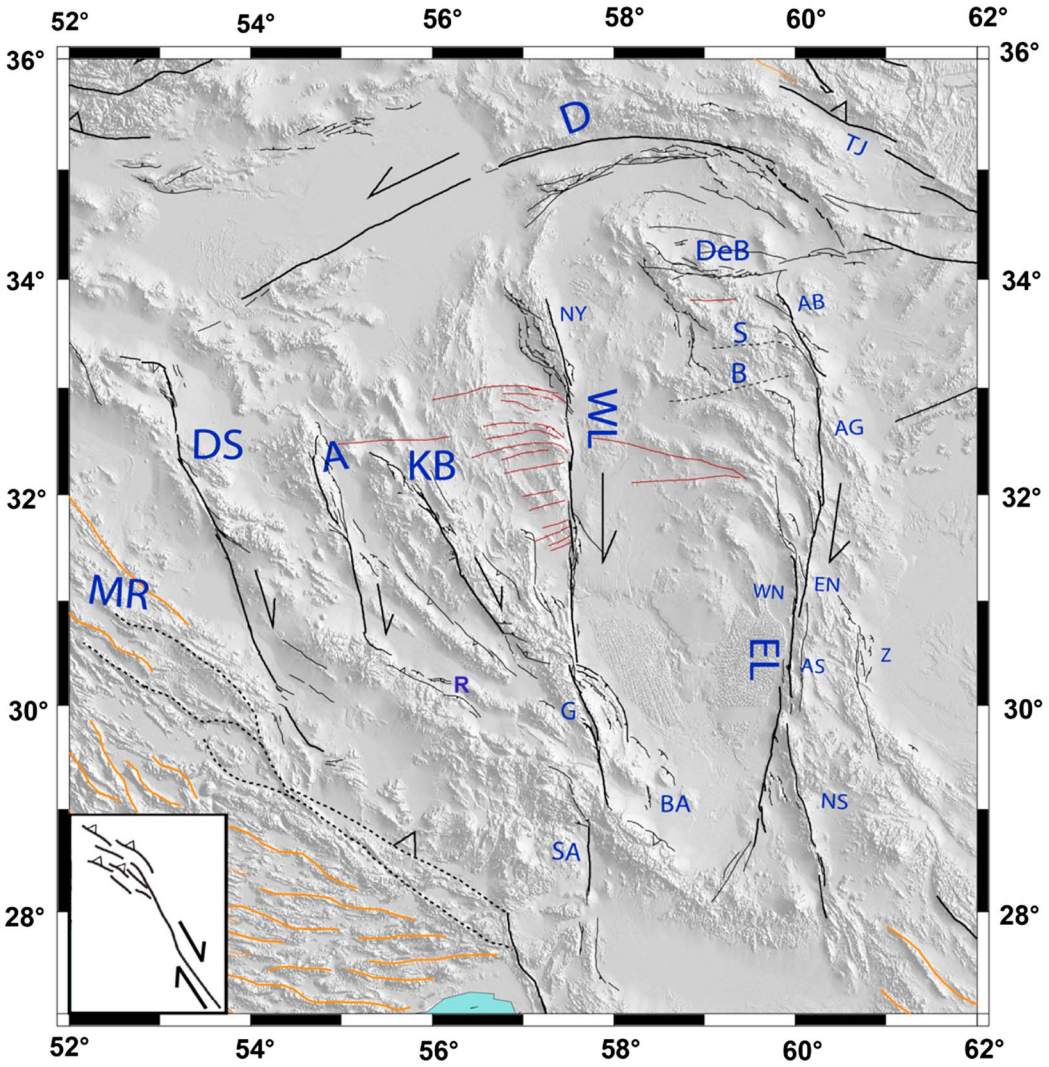

Figure 2. Detailed mapping of major and secondary active faults in eastern Iran. Symbols as in Figure 1. Dotted lines are used for faults for which the morphological evidences of recent activity are subtle or possibly disputable. Brown lines mark old structures. Orange thin lines approximate major fold axes. Note that faults south of MR zone, as faults north of Doruneh, have not been mapped in detail. A: Anar fault; AB: Abiz fault; AG: Avaz-Gazik fault; AS: Asagie fault; B: Birjand fault; BA: Bam fault; D: Doruneh fault; DeB: Dasht-e-Bayaz fault; DS: Dehshir fault; EL: east Lut fault; EN: East Neh fault; G: Gowk fault; KB: Kuhbanan fault; MR: Main Recent fault; NS: Nostarabad fault; NY: Nayband fault; R: Rafsanjan fault; S: Sedeh fault; SA: Sabzevaran fault; TJ: Torbat-e-Jam fault; WL: west Lut fault; WN: West Neh fault; Z: Zahedan fault. Inset sketches compressive horsetail faulting.

morphology [e.g., *Tapponnier and Molnar*, 1976; *McCalpin and Nelson*, 1996]. In transpressional settings as that of eastern Iran, the main indications of recent fault movements are continuous, pronounced, and hence well-preserved traces in the topography and morphology, cutting across or deforming recent morphological "markers" such as active drainage networks, current ground surface and sediment cover, fresh and hence recent alluvial fans, etc. These characteristic morphological features are observed along most of the eastern Iranian faults, allowing the recognition of faults with recent (i.e., late Quaternary) movement, down to structures of ~10 km length. Furthermore, even when they are dominantly strike-slip, most faults in eastern Iran have a minor dip-slip component, which results in the formation of topographic scarps that clearly highlight the fault traces. In Figures 1 and 2, we have mapped the faults that show the clearest morphological evidence of recent movement with thicker traces. The thinner traces are secondary faults that are or that we or other authors suspect to be active, although the morphological evidence might be less clear. Since most of those faults have been described in prior papers, we only provide a few close-up views of their fresh traces in Figure S1 in the supporting information, which we describe in the figure captions.

Figures 1 and 2 show that eastern Iran is dissected by large, active strike-slip faults of two types: N-NW trending, right-lateral strike-slip faults in the central part of the region, and ~E-W trending, left-lateral strike-slip faults in its northern part. In both sets, the major faults are few, while extending over several hundred kilometers in length.

The N-NW striking fault set includes five major right-lateral faults, from east to west, the two ~700 km long, ~ N-S striking faults which bound the Lut block (which, for clarity, we name the east and west Lut faults, EL and WL, respectively; Figures S1a and S1b) [e.g., *Walker and Jackson*, 2004; *Bayer et al*., 2006; *Walker et al*., 2009, 2010]; the NW striking, ~ 300 km long Kuhbanan fault (KB) (Figure S1c) [*Berberian et al*., 1979; *Walker*, 2006; *Allen et al*., 2011; *Walker and Allen*, 2012]; the ~350 km long, NNW striking Anar fault (A) (note that we consider the Anar fault together with the Rafsanjan fault that forms its southern termination) [e.g., *Le Dortz et al*., 2009; *Allen et al*., 2011] (Figure S1d); and the ~500 km long, NNW-striking Dehshir fault (DS) (Figure S1e) [*Nazari et al*., 2009; *Fattahi et al*., 2010]. The east Lut fault is commonly referred to as the Sistan fault and is described as including from south to north the Nostarabad, Asagie, Neh, Zahedan, Avaz-Gazik, and Abiz fault segments [e.g., *Walker and Jackson*, 2004]. The west Lut fault is commonly referred to as the Gowk-Nayband fault, the Gowk and Nayband segments forming the southern and northern parts of the system, respectively [e.g., *Walker and Jackson*, 2004]. The five N-NW right-lateral faults listed above are distant from each other, separated by 150 to 300 km wide regions that are hardly faulted (more details further below). To the south, the longest of these faults end near the main Zagros thrust in the west, while in the east they seem to connect with the thrusts of the Makran accretionary wedge [e.g., *Regard et al*., 2005]. To the north, the three westernmost faults (DS, A, and KB) terminate with no clear connection with other faults, while, in contrast, the Lut-bounding faults abut and possibly connect with oblique structures including E-W faults.

The E-W striking fault set includes one very long, left-lateral strike-slip fault—the ~800 km long, ~ENE trending Doruneh fault (D, also called Great Kavir; Figure S1f) [e.g., *Stocklin and Nabavi*, 1972; *Fattahi et al*., 2007; *Farbod et al*., 2011], and a few shorter ones (100–500 km long), mainly the WNW trending Torbat-e-Jam (TJ) fault north of Doruneh, and the E-W striking Dasht-e-Bayaz (DeB) fault south of Doruneh [e.g., *Walker et al*., 2004]. Two other small faults might exist farther south (Sedeh (S) and Birjand (B) faults, Figure 2) but those do not show any clear morphological evidence of recent activity. Except these two small faults, all ~E-W major faults are active, as recognized in prior studies [e.g., *Walker et al*., 2004; *Walker and Jackson*, 2004; *Walker and Khatib*, 2006; *Hollingsworth et al*., 2006; *Fattahi et al*., 2007; *Farbod et al*., 2011] and confirmed by the close-up views of their traces (Figure S1). The Dasht-e-Bayaz fault recently broke in two large earthquakes ($Mw \sim 7$, 1968 and 1979) [*Ambraseys and Tchalenko*, 1969; *Tchalenko and Berberian*, 1975; *Ambraseys and Melville*, 1982; *Berberian et al*., 1999; *Walker et al*., 2004, 2011]. The faults south of Doruneh are much shorter than those farther north (60–150 km versus $>$300 km, respectively), more closely spaced (30–60 km versus 120–150 km) and confined to a small area enclosed between the northern tip of the east Lut fault and the eastern tip of the Doruneh fault [e.g., *Farbod et al*., 2011]. All together, the ~E-W fault set somehow interrupts the NNW right-lateral faults developed farther south. Farther north, the E-W left-lateral faults give place to the NW trending, right-lateral, and reverse Kopeh Dagh fault zone (Figure 1). The left- and right-lateral motions on the E-W faults and on the Kopeh Dagh fault, respectively, transfer into folding and thrusting east and south of the Caspian Sea [e.g., *Javidfakhr et al*., 2011; *Hollingsworth et al*., 2006, 2008, 2010b].

Most of the secondary faults that we identified are connected to the major faults. The majority of those secondary faults are predominantly reverse, short faults (50–100 km long), associated with folding, that form dense networks at the tips of the master faults (as recognized by *Walker and Khatib* [2006]). Those secondary networks have strikes that are markedly oblique to the mean direction of the principal faults which they connect to. Both the obliquity and slip mode of the secondary faults developed at the master fault tips are in keeping with the sense of lateral motion on those master faults; the secondary networks actually form compressive horsetail terminations to the major faults (Figure 2, inset). The clearest cases are the reverse fault and fold networks developed at both tips of the west Lut fault, but similar horsetail secondary networks have developed at both tips of the DS, KB, and EL faults, as at the southern tip of the A fault and at the eastern tip of the Doruneh fault [*Farbod et al*., 2011]. Some of these secondary oblique faults seem to reactivate preexisting structures [e.g., *Nozaem et al*., 2013; *Walker and Khatib*, 2006]. One clear case is that of the Anar fault, whose southern section (named the "Rafsanjan fault" in *Allen et al*. [2011]) follows a preexisting fold and thrust system.

Secondary oblique, short faults are also observed off the main fault traces which they generally connect to. Again, both the obliquity and slip mode (most are reverse) of those secondary off-fault features are in

keeping with the sense of lateral motion on the major faults. The clearest cases are the reverse, ~NW trending faults and folds developed along the east Lut fault (Figure 2). Some of these oblique, secondary faults may also reactivate preexisting structural trends. This is particularly clear along the west and east Lut faults, where multiple ancient ~ E-W structural trends exist (in brown in Figure 2) [e.g., *Walker and Khatib*, 2006], some of them have probably been reactivated, in particular by the Dasht-e-Bayaz fault. The Sedeh and Birjand faults coincide with some of the ancient features. A few other secondary faults are roughly parallel to the major faults and dissect the regions between the master structures. A few of such faults are observed in the southern regions between the A and KB faults (Jorjafk fault) and between the KB and WL faults (see *Allen et al*. [2011] for more details), and in the northern region between the WL and the EL faults.

Finally, most major faults have their trace divided into a number of major segments, as it is the case of most faults worldwide [e.g., *Manighetti et al*., 2009, 2013], and those segments are generally en echelon arranged, with this arrangement indicating the sense of lateral motion on the main fault. The west and east Lut faults show an especially clear, en echelon segmentation (right-stepping, compressive echelons). We may note that, although they form a single fault zone, those major segments have been generally described as separate faults in the literature (east Neh, west Neh, and Zahedan faults along the EL fault; Nayband, Gowk, and Sabzevaran faults along the WL fault) [e.g., *Walker et al*., 2009]. The en echelon segmentation of the west Lut fault suggests that the fault extends farther south of its "Bam termination," via the Sabzevaran fault, up to the so-called Zendan-Minab fault, where it might connect to the thrusts of the Makran accretionary wedge. The total length of the west Lut fault might thus be up to 800 km. As commonly observed on faults worldwide, dense networks of small, secondary faults have developed in many of the zones that separate the major segments within the faults. Those small secondary faults are oblique to the master fault and are reverse, in keeping with the right-lateral motion on the principal faults. The clearest cases are observed on the A, WL, and EL faults.

Figure 1 shows that the historical and instrumental seismicity underlines most of the faults described above, confirming that those faults are currently active. Some faults or fault sections are, however, free of earthquakes (Dehshir, Anar, central section of the west and east Lut faults and of the Doruneh fault). Conversely, some earthquakes cluster at specific sites along the faults, most of those sites being the fault tips, or zones of fault connection. We will return to these points in the discussion section.

3. GPS Data Acquisition and Processing

The GPS network that we use includes 92 well-distributed stations in eastern Iran (Figure 3). The data cover an 11 year time span (1997–2008), though some cover shorter times (Table 1). They include both campaign and permanent measurements (74 and 18 stations, respectively). The campaign measurements were conducted since 1997 in the framework of the ongoing French-Iranian scientific collaboration, with the support of the National Cartographic Center of Tehran. Most campaign sites are identified with screw markers settled in bedrock. During each campaign, the observation time of each site was at least 48 h. We used Trimble SSE and Ashtech CGRS receivers with choke ring antennas. Note that some of the earliest data have already been used to study the global current kinematics of Iran [*Vernant et al*., 2004a; *Masson et al*., 2007] and the Zagros current deformation [*Tatar et al*., 2002; *Walpersdorf et al*., 2006; *Bayer et al*., 2006; *Tavakoli et al*., 2008]. The temporary measurements are completed with the full time series of permanent GPS data, acquired from both the global permanent IGS network (International GNSS Service [*Dow et al*., 2009]) since 1997 (up to 40 stations), and the Iranian national permanent GPS network (18 stations installed in 2005–2006 in eastern Iran, equipped with Ashtech CGRS receivers and choke ring antennas).

The data analysis is performed with the GAMIT/GLOBK software, version 10.4 [*Herring et al*., 2006]. Following *Vergnolle et al*. [2010], we made a special effort to eliminate the influence of several nontectonic phenomena from the GPS data (troposphere, ocean, and atmospheric loading) in order to enhance the signal to noise ratio and to better measure the tectonic deformation. The daily solutions are combined with the Kalman filter GLOBK to estimate a linear velocity for each site. To obtain realistic velocity uncertainties (Table 1), random walk noise is applied to the site positions. The amount of noise is fixed to 4/4/8 mm^2/yr on the north/east/up components for campaign sites [*Vernant et al*., 2004a], while it is estimated individually for permanent stations according to the measurement time span and the variability of the coordinate time series. This "real-sigma" procedure of the GAMIT/GLOBK software [*Reilinger et al*., 2006] evaluates random walk noise to ~0.1 and 1 mm^2/yr for the horizontal and the vertical position components of permanent stations, respectively.

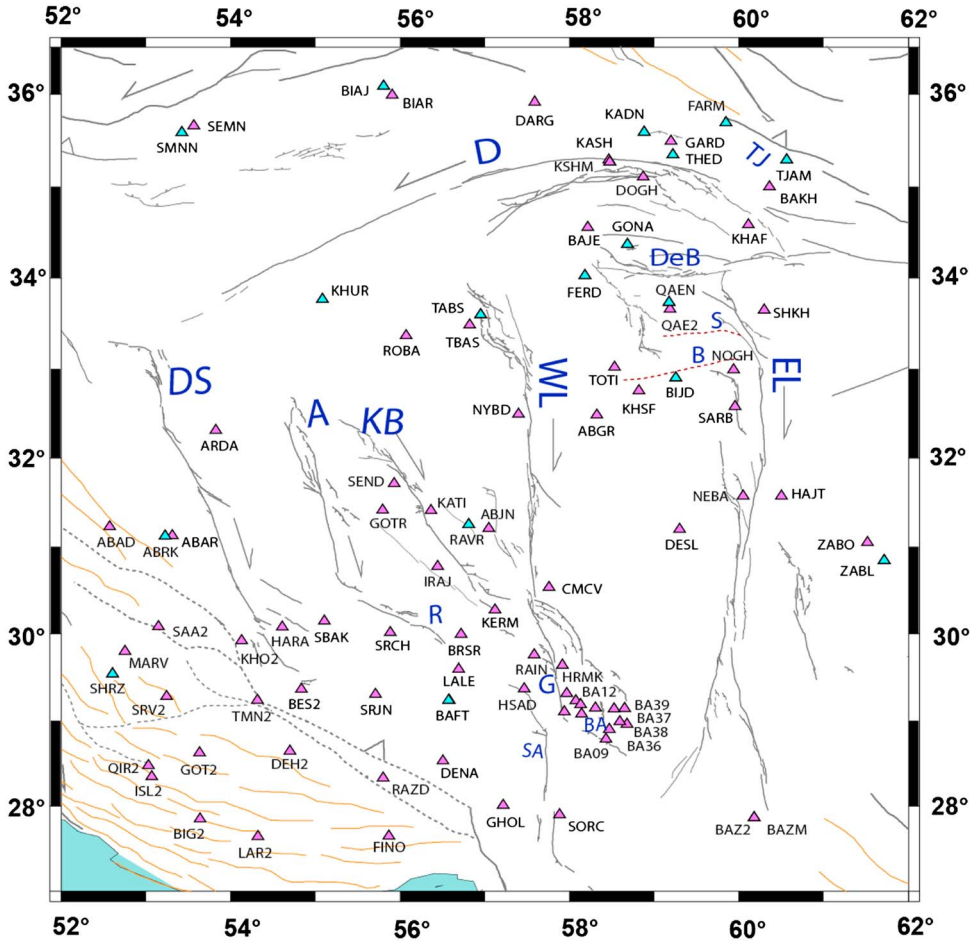

Figure 3. Map of eastern Iranian GPS stations used in our analysis. Blue and pink triangles represent permanent and campaign stations, respectively. Fault names and symbols as before.

We conduct our GPS analysis in the Eurasian reference frame that is established by minimizing the velocities of 17 stations on the Eurasian plate (ARTU, GLSV, GRAS, GRAZ, IRKT, JOZE, KIT3, NYA1, POL2, POTS, SELE, TIXI, TRO1, VILL, WTZR, ZECK, and ZIMM) using a Helmert transformation. The residual velocities (root-mean-square) for these 17 stations are 0.2 and 0.3 mm/yr on the east and the north components, respectively.

4. Approach for Modeling the GPS Data

The GPS data are both dense and broadly distributed and hence can be modeled to estimate the kinematics of present-day deformations in eastern Iran and the current slip rates on most active faults in the zone. For reasons that we explain below, we had to conduct two types of complementary modeling.

Common to any GPS data modeling is the assumption that, in interseismic time, a fault is a planar, locked feature embedded in an elastic medium and sustaining constant strain loading. Under this assumption, dense GPS networks, especially dense transects of GPS stations perpendicular to a fault, can be used to determine simultaneously the current slip rate on the fault and its locking depth [*Savage and Burford*, 1973]. Unfortunately, the 92-station GPS network is still too sparse to build these simple elastic strain accumulation models for most of the faults. Therefore, to estimate the fault slip rates and derive the regional motions, we need to make one additional assumption. This commonly accepted assumption considers that the faults are locked over their entire brittle layer. The crustal thickness in eastern Iran is ~40 km [e.g., *Mooney et al.*, 1998], but the seismogenic thickness is assumed to be lower, ~15 km [e.g., *Maggi et al.*, 2000; *Engdahl et al.*, 2006]. We thus consider that all faults are locked over 15 km.

Table 1. GPS Station Velocities Sorted by Tectonic Unit or Fault[a]

Unit/Fault	Site	Lon	Lat	V_E (mm/yr)	V_N (mm/yr)	sig_{VE} (mm/yr)	sig_{VN} (mm/yr)	Span (years)	# Sol.	Date Midpoint
CIB	**ABAR**	53.308	31.123	−1.93	13.07	0.99	0.98	4.21	5	2006.7265
	ABAD	52.568	31.228	−2.49	13.26	0.99	0.99	4.21	4	2006.6167
	ABRK*	53.226	31.120	−2.12	13.70	1.89	1.89	1.13	16	2006.8417
	KHO2	54.126	29.923	−2.54	14.13	0.91	0.84	5.96	3	2003.7370
	SAA2	53.146	30.087	−2.33	13.31	0.73	0.71	8.94	5	2006.7393
ADB	**ARDA**	53.822	32.313	−1.59	13.26	0.82	0.82	6.02	8	2005.6684
	SBAK	55.107	30.146	−0.42	13.17	1.31	1.31	2.39	3	2007.8833
	SRCH	55.885	30.014	0.14	13.28	1.64	1.63	1.73	2	2007.4111
	HARA	54.608	30.079	0.02	13.07	0.82	0.82	6.02	3	2005.6575
KAB	**GOTR**	55.791	31.416	−0.35	10.63	1.61	1.61	1.73	2	2007.5148
	BRSR	56.721	29.997	−0.12	14.60	1.66	1.65	1.73	2	2007.2530
	IRAJ	56.445	30.775	−0.87	12.89	1.58	1.58	1.73	2	2007.5479
	SEND	55.929	31.713	−0.52	11.75	1.04	1.04	3.87	5	2007.5585
NB	**RAVR***	56.809	31.252	0.43	10.28	0.73	0.69	2.02	62	2008.8125
	ROBA	56.070	33.369	−0.02	9.23	0.67	0.67	9.09	10	2008.6197
	TABS*	56.951	33.603	−0.76	9.15	0.48	0.34	2.26	107	2008.7908
	TBAS	56.819	33.489	−2.98	7.25	1.58	1.58	1.73	2	2007.6196
	NYBD	57.397	32.492	−0.92	8.81	1.25	1.26	2.63	3	2008.6343
	ABJN	57.046	31.206	2.30	10.90	1.62	1.62	1.73	2	2007.6840
	KATI	56.365	31.413	0.55	10.67	1.06	1.06	3.87	5	2007.1043
LB	**DESL**	59.297	31.196	1.33	6.24	1.57	1.56	1.73	2	2007.7681
	BIJD*	59.255	32.900	0.56	6.25	0.40	0.29	2.71	109	2008.8161
	KHSF	58.821	32.755	0.13	5.81	1.15	1.15	3.07	4	2008.6778
	TOTI	58.531	33.019	−0.68	7.40	1.25	1.25	2.63	3	2008.6188
	ABGR	58.319	32.484	0.77	7.09	1.57	1.57	1.73	2	2007.7432
	NEBA	60.047	31.573	0.63	5.27	1.26	1.26	2.63	3	2008.5772
	SARB	59.955	32.578	1.06	4.91	1.16	1.16	3.07	5	2008.6109
	NOGH	59.937	32.988	0.86	4.62	0.98	0.98	4.29	4	2008.6156
	QAE2	59.188	33.663	−0.86	4.23	0.98	0.98	4.29	3	2008.6621
	QAEN*	59.176	33.740	−0.75	4.55	0.35	0.34	2.97	125	2008.8072
	GONA*	58.684	34.373	−0.79	5.38	0.30	0.28	3.15	134	2008.8111
	BAJE	58.215	34.558	−0.53	5.70	0.98	0.98	4.29	3	2008.6643
	FERD*	58.183	34.031	−1.75	7.73	0.38	0.42	2.71	120	2008.8111
	CMCV	57.760	30.537	−0.36	8.20	1.61	1.60	1.73	2	2007.5926
HB	**ZABL***	61.716	30.841	1.71	1.58	1.05	0.77	1.52	61	2008.8319
	ZABO	61.517	31.049	−0.03	1.42	0.67	0.67	9.09	12	2008.5303
	HAJT	60.502	31.573	1.02	1.64	1.15	1.15	3.07	4	2008.7018
	SHKH	60.296	33.654	−0.38	−1.58	1.16	1.16	3.07	4	2007.4672
	BAZ2	60.177	27.865	4.14	2.37	1.42	1.42	2.16	2	2007.6142
	BAZM	60.180	27.865	2.15	3.09	1.44	1.44	6.02	3	2001.6115
NDR	**DARG**	57.589	35.915	−0.76	5.63	0.98	0.98	4.29	4	2008.6307
	GARD	59.197	35.495	−0.22	2.62	0.98	0.98	4.29	3	2008.6919
	KADN*	58.878	35.592	−0.41	2.18	0.80	0.41	3.43	165	2008.8213
	TJAM*	60.564	35.294	−0.51	3.38	0.64	0.68	2.01	61	2008.8449
	BAKH	60.360	35.002	0.08	−0.01	0.98	0.98	4.29	4	2008.6651
	FARM*	59.843	35.696	0.11	1.12	0.39	0.28	3.47	168	2008.7977
	THED*	59.219	35.347	−0.03	3.51	0.28	0.28	3.51	167	2008.7967
	BIAR	55.906	35.988	0.13	8.43	1.17	1.17	3.07	4	2008.5613
	BIAJ*	55.805	36.086	1.30	8.36	0.52	0.37	2.65	74	2008.8303
	SEMN	53.564	35.662	0.38	8.71	0.82	0.82	6.02	3	2005.5872
	SMNN*	53.421	35.588	0.95	8.82	0.39	0.29	3.23	152	2008.6155
SDR	**BAJE**	58.215	34.558	−0.53	5.70	0.98	0.98	4.29	3	2008.6643
	KHUR*	55.081	33.769	−0.14	10.55	0.65	0.48	2.02	60	2008.8472
	DOGH	58.869	35.108	−0.30	4.99	0.98	0.98	4.29	4	2008.6764
S/B	QAE2	59.188	33.663	−0.86	4.23	0.98	0.98	4.29	3	2008.6621
	QAEN*	59.176	33.740	−0.75	4.55	0.35	0.34	2.97	125	2008.8072
	BIJD*	59.255	32.900	0.56	6.25	0.40	0.29	2.71	109	2008.8161
	NOGH	59.937	32.988	0.86	4.62	0.98	0.98	4.29	4	2008.6156
	SARB	59.955	32.578	1.06	4.91	1.16	1.16	3.07	5	2008.6109
DeB	BAJE	58.215	34.558	−0.53	5.70	0.98	0.98	4.29	3	2008.6643
	GONA*	58.684	34.373	−0.79	5.38	0.30	0.28	3.15	134	2008.8111
	QAE2	59.188	33.663	−0.86	4.23	0.98	0.98	4.29	3	2008.6621
	QAEN*	59.176	33.740	−0.75	4.55	0.35	0.34	2.97	125	2008.8072
G	HSAD	57.465	29.371	1.80	13.78	1.56	1.56	1.73	2	2007.7626
	RAIN	57.584	29.762	0.82	13.55	1.55	1.55	1.73	2	2007.7205
	BA07	58.305	29.149	0.91	11.24	1.41	1.41	2.14	6	2005.9876
	BA13	58.074	29.230	0.87	10.37	1.52	1.52	1.92	5	2005.9697
	BA14	57.940	29.105	4.44	9.40	1.04	1.04	3.87	7	2007.4989
	BA30	57.967	29.316	2.94	9.33	1.05	1.05	3.87	7	2007.4277

Table 1. (continued)

Unit/Fault	Site	Lon	Lat	V_E (mm/yr)	V_N (mm/yr)	sig_{VE} (mm/yr)	sig_{VN} (mm/yr)	Span (years)	# Sol.	Date Midpoint
	BA31	58.130	29.187	2.10	10.46	1.45	1.44	2.14	7	2005.6475
	BA32	58.141	29.078	2.25	10.88	1.47	1.46	2.14	6	2005.7444
	BA34	58.278	28.944	3.63	9.28	1.55	1.54	1.92	5	2005.6991
	BA35	58.195	28.888	4.48	10.31	1.48	1.47	2.03	6	2005.6818
	HRMK	57.917	29.642	2.02	9.45	1.57	1.56	1.73	2	2007.7086
BA	BA07	58.305	29.149	0.91	11.24	1.41	1.41	2.14	6	2005.9876
	BA13	58.074	29.230	0.87	10.37	1.52	1.52	1.92	5	2005.9697
	BA14	57.940	29.105	4.44	9.40	1.04	1.04	3.87	7	2007.4989
	BA30	57.967	29.316	2.94	9.33	1.05	1.05	3.87	7	2007.4277
	BA31	58.130	29.187	2.10	10.46	1.45	1.44	2.14	7	2005.6475
	BA32	58.141	29.078	2.25	10.88	1.47	1.46	2.14	6	2005.7444
	BA34	58.278	28.944	3.63	9.28	1.55	1.54	1.92	5	2005.6991
	BA35	58.195	28.888	4.48	10.31	1.48	1.47	2.03	6	2005.6818
	BA12	58.523	29.137	2.60	7.19	1.03	1.03	3.87	8	2007.6660
	BA36	58.469	28.898	2.47	8.41	1.41	1.41	2.14	6	2005.9636
	BA38	58.675	28.960	4.86	6.98	1.04	1.04	3.87	6	2007.5495
	CMCV	57.760	30.537	−0.36	8.20	1.61	1.60	1.73	2	2007.5926
SA	GHOL	57.217	28.010	0.16	14.86	1.44	1.44	1.99	4	2001.9282
	SORC	57.884	27.901	0.94	12.57	1.44	1.43	1.99	4	2001.9530
Not constraining	KHAF	60.110	34.589	−1.38	0.49	0.98	0.98	4.29	4	2008.7051
any unit or fault	KSHM*	58.473	35.271	0.54	4.63	0.30	0.24	3.18	153	2008.7988
	KASH	58.464	35.293	−0.41	4.67	0.82	0.82	6.02	3	2005.6569
	BA09	58.428	28.784	5.17	9.46	1.44	1.44	2.14	6	2005.8341
	KERM	57.119	30.277	0.36	14.90	0.71	0.71	8.18	12	2007.3096
	LALE	56.690	29.596	0.86	14.34	1.06	1.06	3.87	5	2007.7217
	BAFT*	56.580	29.239	0.40	13.27	1.44	1.44	1.73	8	2007.8835
	DENA	56.504	28.529	4.05	14.69	1.45	1.44	1.99	2	2001.9122
	HAJI	55.918	28.302	−6.36	14.24	0.91	0.91	5.21	6	2003.6791
	FINO	55.867	27.651	1.41	19.06	1.47	1.46	1.99	2	2001.8072
	RAZD	55.800	28.330	2.52	14.58	0.85	0.84	5.67	5	2005.6256
	SRJN	55.707	29.304	−0.20	14.38	1.59	1.58	1.73	2	2007.6577
	BES2	54.832	29.363	0.90	13.82	0.91	0.84	5.96	3	2003.6079
	DEH2	54.700	28.645	0.91	13.65	0.89	0.84	5.96	4	2003.7662
	LAR2	54.320	27.644	−0.88	17.64	0.94	0.86	5.96	4	2003.5402
	TMN2	54.316	29.239	1.17	13.53	0.70	0.68	8.94	5	2006.5933
	BIG2	53.637	27.852	1.74	16.05	1.01	0.93	5.96	4	2003.7056
	GOT2	53.631	28.624	1.56	15.67	0.73	0.69	8.94	5	2006.6597
	SVR2	53.244	29.281	1.01	13.58	0.71	0.69	8.94	5	2006.4803
	ISL2	53.066	28.347	1.20	16.30	0.70	0.68	8.94	5	2006.5688
	QIR2	53.029	28.477	1.06	16.00	0.84	0.83	5.96	4	2003.7473
	MARV	52.752	29.798	−0.56	13.44	0.99	0.99	4.21	5	2006.5509
	SHRZ*	52.603	29.544	−1.80	13.76	0.26	0.27	3.00	65	2008.8276

[a]Eight blocks or units and five faults constrained by GPS station velocities: CIB: Central Iran Block; ADB: Anar-Dehshir Block; KAB: Kuhbanan-Anar Block; NB: Nayband Block; LB: Lut Block; HB: Hellmand Block; NDR: North Doruneh Region; SDR: South Doruneh Region. S/B: cumulated Sedeh and Birjand faults; DeB: Dasht-e-Bayaz fault; G: Gowk fault; BA: Bam fault; SA: Sabzevaran fault. Class 1 stations are highlighted by bold letters; permanent stations are indicated by an asterisk. # Sol. indicates the number of campaign solutions or weekly solutions for campaign and permanent sites, respectively.

To simultaneously derive the regional kinematics and the fault slip rates, a classical approach is to use a rigid block model [e.g., *McCaffrey et al*., 2000; *Djamour et al*., 2010; *Mousavi et al*., 2013]. This type of modeling relies on an additional assumption, which is that the major faults accommodate most of the current deformation in the zone under study; in other words, most strain is localized within narrow zones along the major faults, while little deformation is left inside the fault-bounded blocks which may therefore be approximated as rigid and behaving as elastic bodies. The strength of the rigid block model is that it allows all the block motions and the slip rates on the major faults that bound the blocks to be quantified simultaneously. Its weakness is that only major faults that bound large tectonic units can be described, while the secondary faults that might cut the interior of the blocks are ignored. We showed in section 2 that many of such secondary faults exist in eastern Iran and hence should be taken into account in any proper strain modeling. With those limitations in mind, as a first step, we used a rigid block model (Defnode, http://web.pdx.edu/~mccaf/www/defnode/ [*McCaffrey et al*., 2000]) to reproduce the GPS data. We imposed fault locking over 15 km with 100% coupling. This enabled us to include all GPS sites in the modeling: Those at a distance greater than twice the fault locking depth from a fault and whose velocities are expected to represent the rigid block motions (Class 1

Table 2. Euler Pole Estimates, Model Residuals, and Local Rotation Rates of the Major Tectonic Units in Eastern Iran[a]

Unit	N	Model	Lon (°E)	Lat (°N)	Euler Rot. Rate (°/Ma)	Sig. Euler Rot. Rate (°/Ma)	Emax (deg)	Emin (deg)	Az (deg)	Res. (mm/yr)	Local Rot. Rate (°/Ma)
CIB	5	lo	0.2738	11.0664	0.1562	0.1817	80.25	2.00	59.95	0.44	0.094
		fr	351.5830	5.8901	0.1384	0.1380	88.65	2.26	58.60	0.39	0.063
ADB	4	lo	31.2772	28.0670	0.3414	0.2123	18.51	1.22	75.93	0.49	0.319
		fr	26.1311	26.5762	0.2789	0.1937	25.61	1.32	73.34	0.38	0.252
KAB	4	lo	45.6881	29.9378	0.7629	0.5129	8.61	0.70	79.07	1.58	0.754
		fr	38.5907	29.3758	0.4197	0.4872	24.86	1.21	78.83	1.20	0.405
NB	7	lo	42.6500	31.8129	0.4057	0.1617	6.88	0.58	80.81	1.44	0.397
		fr	35.5961	30.4896	0.2710	0.1401	13.63	0.82	77.15	1.41	0.257
LB	12	lo	42.2567	30.9760	0.2158	0.0944	9.00	0.55	75.03	1.41	0.209
		fr	32.6309	28.5806	0.1335	0.0889	22.36	0.88	70.63	1.39	0.123
HB	6	lo	59.2264	32.1358	0.3508	0.1296	1.42	0.88	310.47	1.67	0.351
		fr	58.4797	32.3450	0.3111	0.1250	1.79	0.97	304.01	1.55	0.311
SDR	3	lo	62.8959	34.3467	−0.8268	0.1249	1.15	0.41	269.32	1.17	−0.823
		fr	62.7699	34.3680	−0.8370	0.1300	1.19	0.37	91.39	1.18	−0.834
NDR	11	lo	61.3791	35.4116	−0.7520	0.0326	0.24	0.17	99.17	1.30	−0.751
		fr	61.6382	35.3008	−0.7274	0.0317	0.24	0.16	97.55	1.33	−0.726

[a]N: number of stations on each tectonic unit. Model: lo (locked) or fr (free) faults. Emax, Emin, and Az describe the error ellipse for the emplacement of the pole. Res. is the residuals of horizontal velocities between observations and predictions from the block models. Local rotation rate is the rotation rate about a vertical axis in the center of each block. Tectonic units as in Table 1 and Figure 4.

stations in Table 1), and the many additional stations that are closer to the fault traces and whose velocities are affected by the elastic deformation induced by the fault locking (Class 2 stations in Table 1). Modeling the whole area as a single system of faults and blocks is expected to produce realistic slip rate estimates, including the covariance between slip rates on subparallel faults. The GPS station velocities were used to calculate an Euler pole for each tectonic block (Table 2) and then to derive the average block velocities (Table 3). The relative motions of the blocks inferred from their Euler poles allowed quantifying the slip rates on the major bounding faults. Uncertainties on these rates depend on the uncertainties on the Euler pole locations. These uncertainties can be large, as is the case in the west of the network where GPS vectors are roughly parallel and hence poorly constrain the Euler pole positions (see discussion further below). Intrinsically, since they are derived from block rotations, the modeled fault slip rates are slightly variable along strike. We thus chose to characterize them by their value at the center of the faults (Table 4) and to depict their variability by the rates at the fault tips (Table 5). Finally, we estimated the block "rigidity" by quantifying the fit between the observed and the predicted velocities (residuals in Table 2).

As mentioned above, the existence of many secondary faults in eastern Iran makes the actual strain and slip accommodation more complex than described with a global block model. Therefore, to examine the role of the secondary faults in the overall strain accommodation, we followed a second, complementary modeling approach of the GPS data. This second approach focuses on the fault slip rate evaluation only. It estimates the slip rate on an individual fault by calculating the difference in the average site velocities on either sides of the fault trace (later referred to as the "average velocity method"). Uncertainties on those slip rates are the sum of the dispersions between the site velocities, with the dispersion being calculated as the root-mean-square of the differences of individual site velocities with respect to the average velocity. Where only a single GPS station is available, preventing any dispersion calculation, we use its formal velocity uncertainty.

Table 3. Predicted Tectonic Unit (Block) Velocities at the Center of Each Unit From Block Model With Locked Faults[a]

Unit/Region	V_N (mm/yr)	V_E (mm/yr)	V_{N13} (mm/yr)	V_{N103} (mm/yr)
HB	1.0 ± 0.4	0.8 ± 0.4	1.2 ± 0.4	0.6 ± 0.4
LB	5.9 ± 0.2	−0.2 ± 0.3	5.7 ± 0.2	−1.5 ± 0.3
NB	9.2 ± 0.3	0.1 ± 0.4	9.0 ± 0.3	−2.0 ± 0.4
KAB	13.2 ± 0.8	−1.0 ± 0.8	12.6 ± 0.8	−3.9 ± 0.8
ADB	13.4 ± 0.6	−0.5 ± 0.6	12.9 ± 0.6	−3.5 ± 0.6
CIB	13.6 ± 0.4	−2.4 ± 0.5	12.7 ± 0.4	−5.4 ± 0.5
SDR	7.8 ± 0.4	0.0 ± 0.5	7.6 ± 0.4	−1.8 ± 0.5
NDR	5.2 ± 0.1	0.3 ± 0.2	5.1 ± 0.1	0.9 ± 0.2

[a]The second and third column indicate N and E components, the fourth and fifth column indicate the components in the N13°E AR−EUR convergence direction and in the N103°E perpendicular direction. Components toward N13°E and N103°E are positive. Tectonic units as in Table 1 and Figure 4.

Table 4. Current Fault Slip Rates at the Center of the Major Active Faults in Eastern Iran[a]

			Rigid Block Model			Average Velocity Method			
Fault	Azim	Comp	*Nx/Ny*	Locked (mm/yr)	Free (mm/yr)	*Nx/Ny*	Class 1 (mm/yr)	*Nx/Ny*	Class 1 + 2 (mm/yr)
Dehshir	N162	para.	5/4	1.4 ± 0.9 RL	1.1 ± 0.8 RL	3/2	0.5 ± 0.2 RL	4/3	0.9 ± 0.3 RL
		perp.		−1.3 ± 0.8 EX	−1.2 ± 0.8 EX		−1.1 ± 0.5 EX		0.9 ± 0.3 RL
Anar	N164	para.	4/4	1.2 ±1.3 RL	1.8 ± 1.2 RL	2/1	2.7 ± 1.3 RL		
		perp.		1.3 ±1.0 SH	0.5 ± 1.0 SH		−0.2 ± 1.7 EX		
KBF	N138	para.	4/7	5.0 ± 1.1 RL	3.1 ± 0.9 RL	2/1	2.3 ± 1.9 RL	4/3	2.4 ± 0.8 RL
		perp.		0.9 ± 0.8 SH	1.2 ± 0.9 SH		0.6 ± 1.3 SH		0.4 ± 0.7 EX
West Lut	N000	para.	7/12	4.4 ± 0.4 RL	4.2 ± 0.4 RL	3/4	4.7 ± 1.7 RL	15/10	3.7 ± 1.3 RL
		perp.		0.7 ± 0.7 SH	0.5 ± 0.6 SH		−0.3 ± 0.5 EX		−1.0 ± 1.1 EX
East Lut	N012	para.	12/6	5.6 ± 0.6 RL	5.0 ±0.5 RL	5/4	5.7 ± 0.9 RL	8/6	4.3 ± 0.9 RL
		perp.		−1.4 ± 0.6 EX	−1.7 ± 0.6 EX		−1.4 ± 0.6 EX		−1.8 ± 0.8 EX
Doruneh	N077	para.	11/3	−2.1 ± 0.5 LL	−1.9 ± 0.5 LL	1/2	−0.5 ± 1.1 LL	8/4	0.4 ± 0.3 RL
		perp.		2.1 ± 0.4 SH	1.9 ±0.5 SH		2.6 ± 2.7 SH		1.6 ± 2.1 SH
DeB	N090	para.						2/2	0.2 ± 0.1 RL
		perp.							−1.1 ± 0.3EX
Sedeh/B.	N090	para.						2/3	1.7 ± 0.2 LL
		perp.							0.9 ± 0.6 SH
Gowk	N000	para.						2/9	4.2 ± 0.7 RL
		perp.							−1.4 ± 0.8 EX
Bam	N000	para.						8/4	2.1 ± 1.0 RL
		perp.							0.3 ± 1.7 SH
Sabz.	N000	para.						1/1	2.3 ± 2.4 RL
		perp.							−0.7 ± 2.4 EX

[a]Fault strike is indicated in column 2. Slip rates are given in fault-parallel and fault-perpendicular directions. Block model calculations with locked and freely slipping faults are discriminated. Last four columns (average velocity method) for fault slip rates determined from differences of average GPS velocities to each side of the fault (and not from block model). *Nx/Ny* indicates the number of GPS sites on the western/eastern block or side of the fault for northward trending faults, and on the northern/southern block or side of the fault for eastward trending faults. RL: right-lateral; LL: left-lateral; EX: extension; SH: shortening. KBF: Kuhbanan fault, DeB: Dasht-e-Bayaz fault, Sedeh/B.: Sedeh and Birjand faults; Sabz: Sabzevaran fault.

Though both modeling procedures provide slip rates on the major faults, only the second approach provides slip rates on (some of) the secondary faults. Fault slip on two secondary faults (Sedeh/Birjand and Dasht-e-Bayaz faults) is constrained by station velocities that are used in both the rigid block model and in the average velocity method. Therefore, to verify that slip on those two faults was not counted twice, we re-evaluated the fault slip from the velocity residuals emerging from the rigid block model (using the average velocity method). The slip rates so obtained are similar within uncertainties to those calculated directly from the GPS velocities. Therefore, the slip rates that we evaluated on the Sedeh/Birjand and Dasht-e-Bayaz faults by the average velocity method are not overestimated and are robust.

Table 5. Local Fault Slip Rate Values to Each End of the Major Active Faults in Eastern Iran[a]

		Locked		Free	
Fault	Azimuth	Parallel (mm/yr)	Perp. (mm/yr)	Parallel (mm/yr)	Perp. (mm/yr)
Dehshir N	N102	1.0 ± 1.8 RL	1.1 ± 1.3 SH	0.9 ± 1.8 RL	0.8 ± 1.2 SH
Dehshir S	N133	2.1 ± 0.9 RL	−1.2 ± 1.2 EX	1.8 ± 0.8 RL	−1.2 ± 1.2 EX
Anar N	N015	2.2 ± 1.7 RL	1.3 ± 1.5 SH	2.0 ± 1.8 RL	−0.2 ± 1.4 EX
Anar S	N140	0.6 ± 1.3 RL	0.1 ± 1.7 SH	1.5 ± 1.1 RL	0.6 ± 1.6 SH
KBF N	N121	4.6 ± 1.2 RL	1.8 ± 1.3 SH	2.7 ± 1.0 RL	1.9 ± 1.3 SH
KBF S	N151	5.1 ± 1.1 RL	0.7 ± 1.3 SH	3.3 ± 0.8 RL	0.9 ± 1.2 SH
West Lut N	N356	4.4 ± 0.4 RL	1.4 ± 0.9 SH	4.2 ± 0.4 RL	1.1 ± 0.9 SH
West Lut S	N359	4.4 ± 0.4 RL	0.4 ± 0.4 SH	4.2 ± 0.4 RL	0.3 ± 0.4 SH
East Lut N	N014	5.8 ± 0.7RL	−0.9 ± 0.9 EX	5.2 ± 0.6 RL	−0.9 ± 0.8 EX
East Lut S	N193	5.6 ± 0.6 RL	−2.2 ± 1.1EX	4.9 ± 0.6 RL	−2.6 ± 1.1 EX
Doruneh W	N061	−2.6 ± 0.5 LL	1.9 ± 0.6 SH	−2.3 ± 0.5 LL	1.9 ± 0.6SH
Doruneh E	N109	−0.8 ± 0.6LL	2.7 ± 0.6 SH	−0.7 ± 0.6 LL	2.3 ± 0.6 SH

[a]Slip rates are given in fault-parallel and fault-perpendicular directions. Block model calculations with locked and free faults are discriminated. RL: right-lateral; LL: left-lateral; EX: extension; SH: shortening; KBF: Kuhbanan fault.

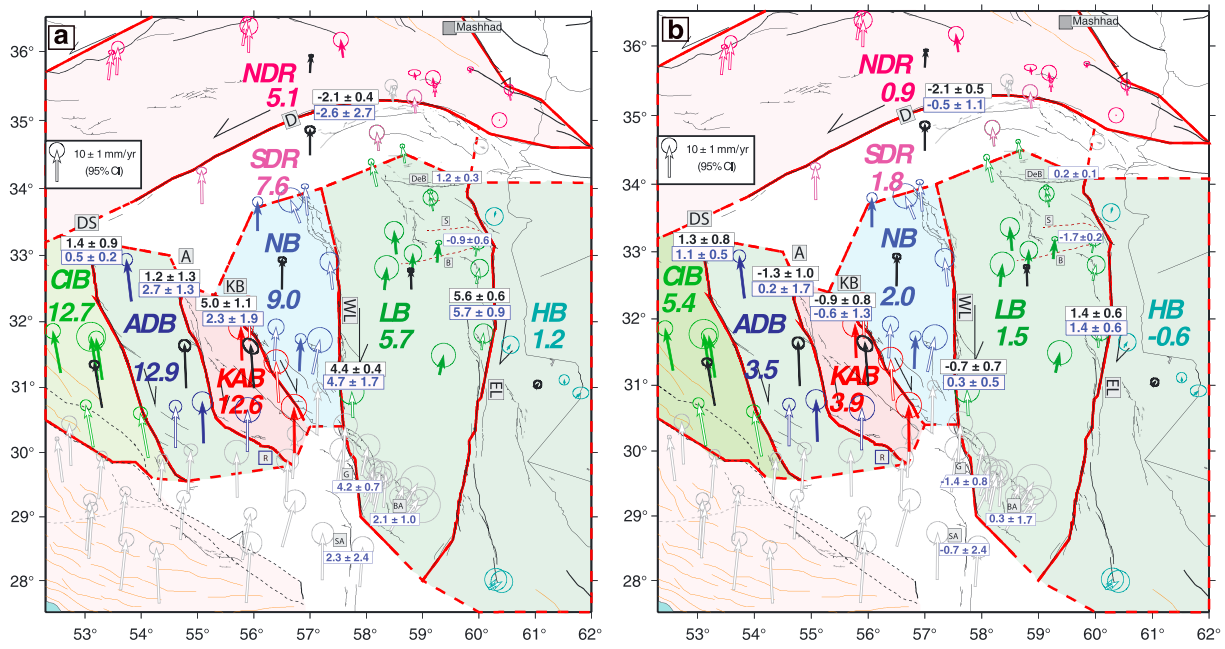

Figure 4. GPS velocity field with respect to Eurasia. The vector error ellipses represent a confidence interval of 95%. Filled vectors indicate class 1 stations, open vectors class 2 stations (see Table 1). Red lines depict the rigid block contours used in the block model with continuous lines where block contours coincide with actual active faults and dashed lines for schematic limits needed to close the block contours. For each block the central velocity obtained from the model is represented by a black vector (Table 3). The block model is used with locked faults. Bold colored numbers indicate the block velocity component in (a) N13°E direction (NNE) and in (b) N77°W direction (WNW). In Figure 4a, with the NNE block velocities, fault-parallel slip is indicated for NS faults (positive values are right lateral), and fault-perpendicular slip is indicated for EW faults (positive values are extension) (Table 4). Black numbers indicate block model predictions; blue numbers are fault slip rates calculated from average velocity method. In Figure 4b, with the WNW block velocities, fault-perpendicular slip is indicated for NS faults, fault-parallel slip for EW faults. Fault velocities from average velocity method are based on class 1 stations only, when available (Table 4). Fault names as in Figure 2 and 3. Major blocks bounded by the faults: CIB: Central Iranian Block; ADB: Anar-Dehshir block; KAB: Kuhbanan-Anar block; NB: Nayband-Kuhbanan block; LB: Lut block; HB: Helmand block; NDR: North Doruneh region; SDR: South Doruneh Region.

5. Present-Day Rigid Block Kinematics in Eastern Iran

The major faults described in section 2 divide eastern Iran into eight principal units, as shown in Figure 4: The Helmand block to the east (HB), bounded by the east Lut fault to the west and the southernmost faults forming the SE end of the Doruneh system in the north; the Lut block (LB) in between the east and west Lut faults; the Nayband block (NB) bounded by the west Lut fault (Nayband section) in the east and the Kuhbanan fault in the west; the Kuhbanan-Anar block (KAB) in between the Kuhbanan and Anar faults; the Anar-Dehshir block (ADB) enclosed between the Anar and Dehshir faults; the "Central Iranian block" (CIB; name from *Vernant et al.* [2004a]) enclosed between the Dehshir and the Main Recent faults; the North Doruneh region (NDR) extending between the Doruneh fault in the south, the Kopeh Dagh in the NE and the Caspian fault system in the NW; and the South Doruneh region (SDR) extending between the Doruneh fault and the northern tips of CIB, ADB, KAB, NB, and LB. Note that the northern ends of the HB, LB, NB, KAB, and ADB units are not exactly defined, as they do not coincide with any clear fault or are the sites of multiple faults. We have thus drawn arbitrary limits made to be in best agreement with the actual faults and to properly enclose the GPS data (Figure 4).

We characterize the motions of the eight units defined above, with respect to fixed Eurasia, by both the velocity inferred from the block model at the center of each unit (i.e., velocity induced by the rotation of the blocks around their Euler pole; Figure 4), and the residual rotation about a vertical axis estimated at the center of each block (Figure 5 and Tables 2 and 3).

Bold numbers in Figure 4 show the block velocities calculated with respect to the AR-EUR convergent motion vector at the mean longitude of eastern Iran (~N13°E direction at Hormuz, e.g., *Masson et al.* [2007]) (Table 3), that is, in both the N13°E (Figure 4a) and in the perpendicular N103°E directions (Figure 4b) (later referred to as NNE and WNW directions, respectively). In Figure S2, we quantify the block velocities in the classical NS/EW reference frame.

The block motion "residuals" are reported in Table 2. Residuals are taken as the differences between observed and modeled values. Those differences result mainly from the errors in assumed locking depth

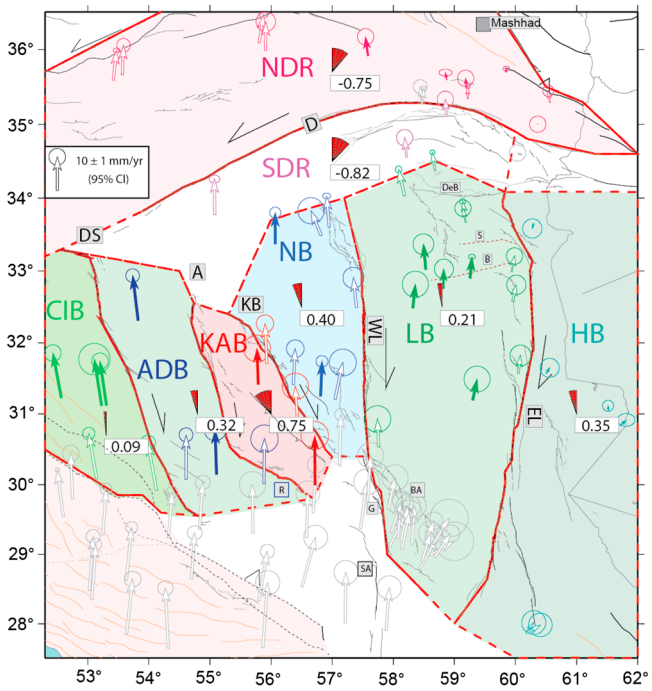

Figure 5. GPS block rotation rates in °/Ma measured in the center of each block (from block model with locked faults) (Table 2). Counterclockwise rotation sense is positive. Faults and blocks as before.

and degree of coupling of the major faults, and from the deviation from the strictly rigid block hypothesis. The rigid block hypothesis is the factor that most controls the differences between observation and model, and therefore the uncertainties of the model parameters. The two westernmost blocks, CIB and ADB, have small residuals, 0.4 and 0.5 mm/yr, respectively, indicating that the rigid hypothesis, locking depth, and coupling are correct for these blocks (within the limit of resolution of the available GPS data). On the contrary, both NDR and SDR units have large residuals, 1.2 and 1.3 mm/yr, respectively, and we suspect that those large residuals mainly result from the dense secondary faulting that dissects the two units and makes them far from being rigid [e.g., *Farbod et al.*, 2011]. The KAB, NB, LB, and HB units also have fairly large residuals. Those might result from the block motions being inferred from many stations close to the faults. It is also likely the KAB, NB, and LB blocks are not fully rigid, due to the numerous secondary faults that cut them (Figure 2). Furthermore, 4 out of 11 stations that were used to model the Lut Block are located north of the Birjand fault, in an area showing dense secondary faulting. Finally, only four stations are used to model the KAB block, two of them within the deformation zone close to the fault, whereas the block is cut by a clear secondary fault, the Jorjafk fault. The KAB is thus the less well constrained unit in our data.

However, in all cases, the residuals are lower than the slip rates that we estimate on the major bounding faults (see next section and Figure 4). The GPS data thus confirm that each fault-bounded tectonic unit behaves in a fairly rigid fashion, and hence as a block. All blocks move both toward the north and toward the west (with the exception of HB). The NNE rates are fast with respect to Eurasia, ranging from ~ 1 to 13 mm/yr (Figure 4a). The WNW rates are slower, in the range ~ 1–5 mm/yr (Figure 4b). Taken together, our measurements reveal an overall increase in the NNE velocity from the HB in the east to the CIB in the west, together with a slight increase in the WNW motion. The increase in the NNE velocity occurs in a step fashion across the EL, WL, and KB faults, while the NNE velocity is roughly the same for the KAB, ADB, and CIB blocks (12.5–13 mm/yr; see also Figure S3). The variation in the WNW velocity shows a similar evolution, but step increases occur across the KB and DS faults (see also Figure S3).

The rotations of the blocks about a vertical axis are calculated at their center and reported in Tables 2 and 6 and in Figure 5. All N-S blocks are found to rotate counterclockwise at rates ranging from 0.1 to 0.8°/Ma. The lowest counterclockwise rotation rate is found for CIB, as a result of the subparallel GPS velocities on this

block. The NDR and SDR regions sustain clockwise rotations at rates of 0.7–0.8°/Ma. Those rotations are controlled by the progressive increase in GPS velocities from east to west over the large E-W extent of the NDR and SDR regions. As those two regions do not represent rigid tectonic units [e.g., *Farbod et al*., 2011] (Figure2), the clockwise rotation rates calculated from the block model should be interpreted with caution.

To estimate the robustness of the block velocities and rotations, we calculate an alternative model with freely slipping faults. The two extreme models—one where faults are 100% coupled and one where faults are freely slipping—provide extreme values of the possible block velocities, rotations (Table 2), and fault slip rates (Tables 4 and 5). We derive the uncertainties on the block velocities, rotations and fault slip rates from the variability of those two parameters among the two calculations. Calculated in this way, it is likely that the uncertainties stand at the highest range of the actual uncertainties and hence are large enough to capture the various sources of errors that affect the calculations (rigid hypothesis, locking depth, degree of coupling). The block velocities and rotation rates and the fault slip rates that we infer are thus robust within those large, conservative uncertainties.

6. Current Slip Rates on Eastern Iranian Faults, and Comparison With Long-Term Rates

6.1. Current Slip Rate Calculations

For the reasons explained before, we estimate the current fault slip rates using two approaches: (1) the block model, in which the slip rates are deduced from the comparison of the rigid motions of the blocks on either sides of the major fault traces; and (2) the calculation of the differences between average GPS velocities on either sides of the fault traces (the average velocity method). While the block model permits a coherent fault slip rate distribution to be established over the entire network, it estimates slip rates on the major faults only. Meanwhile, although the average velocity method enables the slip rates on some of the secondary faults to be estimated, it neglects the motions caused by the rigid block rotations. The two approaches are therefore complementary and their comparison is an opportunity to quantify the uncertainties on the fault slip rates.

As described before, we use Defnode to test two extreme hypotheses, one more realistic, with 100% of fault locking, and one unlikely, with freely slipping faults. The differences between the two extreme solutions provide a fair evaluation of the uncertainties on the fault slip rates. The rates evaluated at the center of the faults and their uncertainties are reported in Table 4 and shown in Figure 4, while the rates estimated more locally along the faults are listed in Table 5 and shown in Figure S4. The largest differences between the two extreme solutions, and hence the largest uncertainties, are found for the slip rates of the Kuhbanan (1.9 mm/yr on the right-lateral component, exceeding the formal error limit) and the Anar faults (0.8 mm/yr of across-strike shortening, but within the formal error limits) that both bound the KAB block. Those large uncertainties on both fault slip rates probably result from the imperfect description of the KAB motion by the rigid block model (see discussion in section 5). The formal uncertainties on the other fault slip rates, generally of 0.5 mm/yr, are larger than the differences between the two extreme solutions and are therefore likely to be robust. We retain the rigid block model with locked faults that provides, in the rigid block model framework, the most robust fault slip rates and uncertainties, and that represents a more realistic fault description.

The second approach to quantify fault slip rates is based on the elastic deformation model of *Savage and Burford* [1973], where the deformation field across a locked fault recovers the total fault slip rate at distances of about twice the locking depth. With this assumption, the GPS sites located at a distance greater than twice the fault locking depth from a main fault trace (30 km here) and not obviously affected by other adjacent faults, can be used to derive a slip rate on that fault. These most appropriate sites (referred to as Class 1) are highlighted in bold in Table 1. Many additional stations exist, which are either closer to a main fault trace, or in between secondary adjacent faults, and hence are possibly slightly perturbed by these faults (referred to as Class 2). Together, these make us perform two calculations (Table 4). In a first step, wherever possible, we derive a slip rate on each fault from using only the Class 1 GPS data. This slip rate is thus derived from fewer but rigorously selected sites. In a second step, we combine the Class 1 and Class 2 data to derive a slip rate on each fault that is constrained by a larger number of stations, although some of them might show some perturbations. Comparison of fault slip rates based on Class 1 stations only and on Class 1 and 2 stations together shows that, in most cases, the slip rates estimated by including the Class 2 stations are lower than the slip rates based on the Class 1 stations only. This is in keeping with the Class 2 stations generally being close to the fault trace, and hence being in the zone expected to sustain elastic strain. This result confirms

that our classification of the sites is appropriate, and that the slip rates estimated from the Class 1 stations are the best constrained, and hence those are to be retained when they exist.

For the six major faults (DS, Anar, KB, WL, EL, and Doruneh), we can compare the slip rates obtained with the two approaches (Table 4). Generally, the actual sense of fault slip is appropriately recovered with the two techniques. The slip rates are similar for the WL, EL and DS faults (within ± 1.0 mm/yr for both fault parallel and fault perpendicular components). We showed that the KAB unit is poorly represented by a rigid block. This might explain why the two methods provide significantly different slip rates on its two bounding, Anar and KB faults. While the block model attributes a high right lateral slip rate on KB (5.0 ± 1.9 mm/yr) and a weak slip rate on Anar (1.2 ±1.3 mm/yr), the other method yields more balanced values with 2.3 ± 1.9 mm/yr and 2.7 ± 1.3 mm/yr of right-lateral slip on KB and Anar, respectively. Furthermore, while the block model predicts shortening across the Anar fault (at 1.3 ± 1.0 mm/yr), the second approach does not suggest any significant across-fault deformation (−0.2 ± 1.7 mm/yr). More GPS data in the central part of the KAB unit are clearly necessary to determine which slip rates are more realistic on the Kuhbanan and Anar faults. The Doruneh fault also shows fairly different slip rates depending on the approach. While both approaches conclude to a similar across strike shortening of 2.1–2.6 mm/yr, the block model predicts a higher left-lateral slip rate (−2.1 mm/yr) than the average velocity method (−0.5 mm/yr). None of the two approaches seems to be satisfying. On the one hand, the NDR and SDR regions are clearly densely offset by secondary faults and hence cannot be appropriately described as rigid units. On the other hand, due to the great length of the Doruneh fault, the average velocity approach neglects a significant component of rotation in the estimation of the fault parallel slip rate. Our data thus only reveal that the Doruneh fault is sustaining about 2 mm/yr of across-strike shortening. Its left-lateral strike slip rate is weakly constrained in the range 0.5-2.1 mm/yr.

In conclusion, both approaches yield similar fault slip rates, with only few exceptions. For those we retain that their slip rate is in the range of the values provided by both methods. For all the other faults, we retain the slip rates estimated from the block model (i.e., for major faults), to which we add the secondary fault slip rates estimated from the average velocity method.

6.2. Current Fault Slip Rates and Comparison With Long-Term Slip Rates

Here we present the current slip rates estimated from the GPS data on the major active faults in eastern Iran (Tables 4 and 5). Moreover, we synthesize the information available in the literature on the long-term history of the faults, including their initiation age, maximum cumulative slip, and Holocene slips rates. All these parameters are compiled in Table 6 where the long-term slip rates can be compared to our current slip rate estimates.

6.2.1. East Lut Fault System

This is the first time that the east Lut fault slip rate can be estimated in isolation from that on the west Lut fault. The differential motion of the HB and LB blocks results in a right-lateral slip operating at 5.6 ± 0.6 mm/yr along the east Lut ~ N12°E mean strike. An additional, fault-perpendicular component of extension is revealed, operating at a rate of 1.4 ± 0.6 mm/yr. The right-lateral slip rate is roughly constant along the fault, ranging from 5.6 ± 0.6 mm/yr in its southern part to 5.8 ± 0.7 mm/yr in the north.

Over the long-term, the east Lut fault is taken to have accumulated up to 95 km of lateral slip (when considering the overall fault system including the eastern Zahedan fault, Figure 2) since its onset of activity [*Walker and Jackson*, 2004; *Meyer and Le Dortz*, 2007], a time not well established, but estimated to be at most 12–20 Ma. Lateral offsets of 40–60 m have been measured in river channels of assumed Holocene age [*Meyer and Le Dortz*, 2007]. If the channel incision occurred in the Holocene optimum [*Le Dortz et al*., 2009], the Holocene slip rate on the east Lut fault is 8 ± 4 mm/yr. Therefore, the current slip rate on the east Lut fault (5.6 ± 0.6 mm/yr) is on the same order within uncertainties than its Holocene rate.

6.2.2. West Lut Fault System

The GPS-inferred LB and NB differential motion induces a roughly constant 4.4 ± 0.4 mm/yr right-lateral slip rate on the west Lut fault. An across-strike shortening component also exists that averages 0.7 ± 0.7 mm/yr and increases from 0.4 ± 0.4 mm/yr in the north to 1.4 ± 0.9 mm/yr in the south. Altogether, these are the first velocity estimates that distinguish the fault systems to the east and to the west of the Lut block. Our results highlight that the west Lut fault slip rate is similar to the current slip rate on its companion east Lut fault.

Total geological slip of the west Lut fault is estimated to be a minimum of 15 km (measured on its southern Gowk segment) [*Walker and Jackson*, 2002]. The initiation age of the fault is unclear. From the measurement

of morphological offsets whose ages were assumed to be 5–8 Ma, a long-term slip rate of 1.5–2.5 mm/yr was estimated [*Walker and Jackson*, 2002]. More recently, *Walker et al*. [2010] estimated a Holocene slip rate of 3.8 ± 0.7 mm/yr on the Gowk segment of the WL fault, and a 2.2 Ma slip rate of 1.4 ± 0.5 mm/yr on its Nayband segment. *Regard et al*. [2005] estimated a late Quaternary slip rate of 5.7 ± 1.7 mm/yr on the southern Sabzevaran-Jiroft fault. The current slip rate that we find on the WL fault is 4.4 ± 0.4 mm/yr, with local estimates of 4.2 ± 0.7 mm/yr on the Gowk fault segment, 2.1 ± 1.0 mm/yr on the Bam fault segment, and 2.3 ± 2.4 mm/yr on the Sabzevaran fault segment. The current and long-term slip rates of the west Lut fault are thus fairly similar within uncertainties.

6.2.3. Kuhbanan Fault

The differential motion of the NB and KAB blocks yields a present-day right-lateral slip rate of 5.0 ± 1.9 mm/yr on the N140°E mean strike of the KB fault, and an across-strike shortening of 0.9 ± 0.8 mm/yr. However, as discussed in section 6.1, the lateral slip rate might rather be in the range 2.3–5.0 mm/yr and hence be of the order of 3.6 ± 1.3 mm/yr. The lateral slip rate seems to vary along-strike, increasing from NW to SE.

The Kuhbanan fault is taken to have slipped laterally by a minimum of 20 km over a period of time that is unknown but likely to be similar to the other faults, 12-20 Ma [*Allen et al*., 2011] (the offset has been measured on the Dehu fault which is part of the Anar fault zone). From a few cumulative slip measurements with estimated ages, a poorly constrained Holocene slip rate is suggested around 1.5 mm/yr [*Berberian et al*., 1979; *Talebian et al*., 2006; *Allen et al*., 2011]. The GPS measurements imply that the fault is presently active and possibly slipping faster than over the Holocene and geological times.

6.2.4. Anar Fault

The Anar fault current slip rate is evaluated from the KAB and the ADB motions. We estimate 1.2 ± 1.3 mm/yr of right-lateral slip on the fault and 1.3 ± 1.0 mm/yr of shortening across its strike. Yet as discussed in the previous section, the lateral slip rate might rather be in the range 1.2–2.7 mm/yr (hence 2.0 ± 0.7 mm/yr), while the across-strike motion might not be well constrained. In the block model solution, both lateral and across-strike slip rates increase from south to north.

Over geological times, the Anar fault is taken to have slipped laterally by a minimum of 30 km over the last 20 and more likely 12 Ma [*Walker and Jackson*, 2004; *Meyer and Le Dortz*, 2007]. From the measurement and dating of offset stream risers, a minimum Holocene slip rate of 0.8 mm/yr is inferred at one central site of the fault [*Le Dortz et al*., 2009]. The long-term and Holocene slip rates on the Anar fault might thus range between 0.8 and 1.5 mm/yr. The current right-lateral slip rate is evaluated to 1.2–2.7 mm/yr, thus in a fairly similar range.

6.2.5. Dehshir Fault

The ADB and CIB relative motion constrains 1.4 ± 0.9 mm/yr of right-lateral present-day slip rate on the Dehshir fault and 1.3 ± 0.8 mm/yr of fault perpendicular extension. Both the right-lateral and extensional slip rates seem to increase from NW to SE.

The Dehshir fault is supposed to have slipped laterally by up to 80 km over the last 20 Ma [e.g., *Walker and Jackson*, 2004; *Meyer et al*., 2006; *Nazari et al*., 2009] and more likely 12 Ma [e.g., *Sengor and Kidd*, 1979; *Sengor*, 1990; *Allen et al*., 2004]. A minimum late Quaternary slip rate of 0.8–2.5 mm/yr is estimated at one central site of the fault from the measurement and dating of offset stream channels [*Nazari et al*., 2009]. If the incision has occurred in the Holocene optimum (8 ± 2 kyr) [*Le Dortz et al*., 2009], the Holocene slip rate on the Dehshir fault would rather range between 2.5 and 4.2 mm/yr. Recent slip and age measurements at two nearby sites of the fault suggest a late Quaternary slip rate of 1.2 ± 0.3 mm/yr [*Le Dortz et al*., 2011]. Therefore, according to available data, the Dehshir fault might have slipped at 0.8–4.2 mm/yr, and hence at 2.5 ± 1.7 mm/yr over the late Quaternary. The current right-lateral slip rate that we estimate averages 1.4 ± 0.9 mm/yr and hence is in the range of the geological estimates.

6.2.6. Doruneh Fault

The GPS stations in the SDR and the NDR regions are both sparse (only three stations on SDR) and unevenly distributed, with most of them located in the east. Furthermore, the Doruneh fault strike markedly varies along its length, bending from ~ E-W in its eastern part to ~ N60°E in its western half. As a consequence, the current lateral slip rate on the Doruneh fault is not well constrained yet. We find it to be in the range 0.5–2.1 mm/yr on the average N077°E strike of the fault (Figure 4b). Additionally, it might vary along the fault from 2.6 ± 0.5 mm/yr in the west to 0.8 ± 0.6 mm/yr in the east. The relative NDR and SDR motion more robustly constrains a fault perpendicular shortening of 2.1 ± 0.4 mm/yr (Figure 4a). The across-strike compressive component slightly increases toward the east.

The cumulative slip on the Doruneh fault is unknown, as is its initiation age [e.g., *Farbod et al*., 2011]. On the basis of a simple model, *Walker et al*. [2004] suggest that the Doruneh fault might have slipped at 2.5–10 mm/yr over the long-term. From the measurement and the dating of one offset alluvial terrace at one fault site, a local Holocene slip rate of 2.4 ± 0.3 mm/yr is estimated [*Fattahi et al*., 2007], reaching ~3.0 mm/yr at a nearby site (R. Walker, personal communication, 2012). The current and Holocene Doruneh lateral slip rates are thus in the same range. Additionally, our GPS measurements evaluate a significant component of across-strike shortening on the Doruneh fault.

6.2.7. Slip Rates on Secondary Faults

6.2.7.1. Dasht-e-Bayaz Fault

Four stations are used to evaluate the Dasht-e-Bayaz fault slip rate to a NS extension of 1.2 ± 0.3 mm/yr combined with an EW lateral slip of 0.2 ± 0.1 mm/yr, yet being dextral while the fault is unambiguously left-lateral (two $Mw \sim 7$ events in 1968 and 1979 on the fault) [*Ambraseys and Tchalenko*, 1969; *Tchalenko and Berberian*, 1975; *Ambraseys and Melville*, 1982; *Berberian et al*., 1999; *Walker et al*., 2004, 2011]. Large wavelength and long lasting postseismic displacements induced by the large earthquakes that occurred in the area in 1997 (Zirkuh earthquake on nearby Abiz fault), 1979, and 1968 might explain this discrepancy but testing this hypothesis is beyond the scope of the present study. Therefore, currently, we cannot explain the discrepancy between the actual sense of slip and that observed in the GPS data. Our data only suggest that the current left-lateral slip on the Dasht-e-Bayaz fault is likely to be small.

A minimum Holocene left-lateral slip rate of 2.5 mm/yr is estimated on the western section of the Dasht-e-Bayaz fault from the lateral offset of ancient man-made features [*Berberian and Yeats*, 1999]. The cumulative lateral offset on the fault is taken to be at most a few kilometers [*Walker et al*., 2004], while the fault initiation age is unknown. While the GPS measurements evaluate a slower current slip rate on the Dasht-e-Bayaz fault itself, other nearby secondary faults exist that might absorb a present-day motion of the order of the Dasht-e-Bayaz Holocene slip rate: The Sedeh and Birjand faults some 80 km farther south.

6.2.7.2. Sedeh and Birjand Faults

It is noteworthy that the GPS data constrain some current slip in a region where there exists only two small EW trending faults due south of Dasht-e-Bayaz, the Sedeh and Birjand faults, whose morphological signature does not reveal any clear recent activity (Figure 2). According to the GPS data, those faults are candidates to accommodate together a significant left-lateral motion, at a rate of 1.7 ± 0.2 mm/yr, associated with a northward compression operating at 0.9 ± 0.6 mm/yr. This is the first time that these faults are suggested as active structures. Further work is deserved to validate their seismogenic activity, and to determine whether the current motions that we observe along those secondary faults characterize their interseismic behavior or reflect large wavelength and long lasting postseismic deformations induced by nearby historical earthquakes as those that occurred in the Dasht-e-Bayaz area.

6.2.7.3. Gowk, Bam, and Sabzevaran

The available GPS stations allow the current right lateral slip rate on the Gowk fault, 4.2 ± 0.7 mm/yr, to be isolated from that on the Bam fault, 2.1 ± 1.0 mm/yr. Note that these rates are estimated from the GPS stations that were not affected by the 2003 Bam earthquake, and hence are likely to be robust, though we cannot preclude that postseismic deformation might affect them. Farther south, the west Lut fault system continues into the Sabzevaran fault, whose current right-lateral slip rate is estimated at 2.3 ± 2.4 mm/yr.

Walker et al. [2010] estimated a Holocene slip rate of 3.8 ± 0.7 mm/yr on the Gowk fault, whereas *Regard et al*. [2005] evaluated a late Quaternary slip rate of 5.7 ± 1.7 mm/yr on the southern Sabzevaran-Jiroft fault. The Gowk and Sabzevaran fault segments that form the southern part of the west Lut fault system have thus each been slipping at a similar rate (within uncertainties) over the Holocene up to present.

The comparative analysis of our present-day fault slip rates thus shows that the eastern Iranian faults are currently slipping at fast rates that are fairly similar to those they had in the Holocene and possibly over longer time spans.

7. Interpretation and Discussion

7.1. Accommodation of Current Strain in Eastern Iran

For the first time, the GPS data demonstrate that the six major faults that dissect eastern Iran, east Lut, west Lut, Kuhbanan, Anar, Dehshir, and Doruneh, are all currently active, as attested by their morphological

Table 6. Test of the Vertical Axis Block Rotation Model Using the Fault Characteristics and Slip Rates Discussed in the Text[a]

		Measures and Estimates From This Study and Literature						
Block Name	Fault Name	Age of Eastern Fault (Ma)	L (km)	W_b (km)	Measured Long-Term Slip S_L (km)	Measured Holocene Slip Rate S_H/yr (mm/yr)	Estimated Current GPS Fault Slip Rate S_C/yr (mm/yr)	Estimated Current GPS Rotation Rate (°/Ma)
CIB	MR and **Dehshir**	12–20	~ 470	~ 200	80	2.5 ± 1.7	1.4 ± 0.9	0.1
ADB	Dehshir and **Anar**	12–20	~ 380	~ 150	> 30	> 0.8	1.2–2.7	0.3
KAB	Anar and **Kuhbanan**	12–20	~ 300	~ 150	> 20	~ 1.5	2.3–5.0	0.8
NB	Kuhbanan and **West Lut**	12–20	~ 700	~ 200	*>> 15*	3.8 ± 0.7	4.4 ± 0.4	0.4
LB	West Lut and **East Lut**	12–20	~ 700	~ 300	95	8 ± 4	5.6 ± 0.6	0.2
								0.4 ± 0.25

[a]Column 1: Block names as in Figure 4. Column 2: Names of corresponding bounding faults. Eastern fault in bold, for which all calculations are done. Column 3: Age of initiation of the faults, in Ma, as inferred from literature (see text). Column 4: Length L of the faults, in km (from Figure 2). Column 5: Width W_b of the rotating blocks, in km (from Figure 2). Column 6: Cumulative lateral slip on eastern bounding fault, in km, as reported in literature (see text). Column 7: Holocene right-lateral slip rate S_H/yr on eastern bounding fault, in mm/yr, as reported in literature. Column 8: Current GPS right-lateral slip rate S_c/yr on eastern bounding fault, in mm/yr, estimated in the present study. Column 9: Current block rotation rates, in °/Ma, estimated from the GPS data (rigid block model with locked faults). For uncertainty, see Table 2 and text. Column 10: Total rotation in degrees inferred over the long-term from the vertical axis block rotation model. Column 11: Long-term rotation rates, in °/Ma, inferred from the vertical axis block rotation model. Column 12: Holocene rotation rates, in °/Ma, inferred from the vertical axis block rotation model. Column 13: Current rotation rates, in °/Ma, inferred from the vertical axis block rotation model. Column 14: Current eastward or westward velocity estimated from the vertical axis block rotation model for the tips of the rotating faults (see Figure S4). In bold at bottom are average values. See text for more details.

traces (section 2). We provide the first estimates of the present-day slip rates on these faults (Figure 4). The three easternmost faults, EL, WL, and probably KB, have the fastest along-strike slip rates in the range 4–6 mm/yr, whereas all the other faults have lower slip rates in the range 1–3 mm/yr (Table 4). Our slip measurements furthermore confirm that the five major northerly striking faults that dissect eastern Iran are dominantly right-lateral, while the Doruneh fault is left-lateral, slipping at 0.5–2.5 mm/yr.

Though the eastern Iranian faults are dominantly strike-slip, they also show an additional component of across-strike motion. This motion is extensional on the two outermost faults, DS and EL, and compressional on all the other faults, including Doruneh. In all cases, the across-strike motion operates at a rate of ~ 0.5–2 mm/yr (Table 4).

The tectonic units bounded by the major ~ NS faults behave as quasi-rigid blocks that are all found to rotate counterclockwise about a vertical axis, at rates ranging from 0.1 to 0.8°/Ma and averaging 0.4 ± 0.25°/Ma (Table 6). By contrast, the SDR and NDR regions sustain clockwise rotations at a rate of ~ 0.8°/Ma (Figure 5). This clockwise rotation is not strongly constrained, however, since neither the NDR nor SDR region is a rigid block over its overall, large E-W extent.

All tectonic units and blocks move toward the N13°E direction at fast rates with respect to Eurasia, ranging between ~ 1 and 13 mm/yr (Figure 4a). Although the overall NNE motion decreases northward across the major faults, as those accommodate part of it, it remains elevated north of the northerly striking fault set, of the order of 8 mm/yr due south of Doruneh, and 5 mm/yr north of it. The total NNE shear between Central Iran (represented by the westernmost CIB block) and Eurasia (represented by the HB block) is 11–12 mm/yr. Though large, this value is smaller than previous suggestions (16 mm/yr) [*Vernant et al.*, 2004a]. The NNE shear is absorbed successively by the major N-S faults, each of the east Lut, west Lut, and Kuhbanan faults accommodating about 25–40% of that shear.

In addition to their overall NNE motion, all northerly trending blocks move toward the WNW with respect to Eurasia, at significant rates varying from ~ 1 to 5.5 mm/yr from east to west (Figure 4b).

7.2. Accommodation of the North-South Convergence in Eastern Iran

7.2.1. The GPS Data as a Test of the Possible Models

Our data shed light on the way faults in eastern Iran accommodate the overall north–south convergence between Arabia and Eurasia. The question is pertinent, as most major faults in eastern Iran strike approximately parallel to the convergence vector, and hence cannot accommodate the convergence in a simple way (i.e., convergence-perpendicular thrusting and folding). This situation has motivated many authors to suggest different models of fault and deformation kinematics across eastern Iran [*Jackson and McKenzie*, 1984; *Walker et al.*, 2004; *Walker and Jackson*, 2004; *Allen et al.*, 2006, 2011; *Walker and Khatib*, 2006; *Hollingsworth et al.*, 2010a]. However, until now, those models were lacking data, especially current motion data, to validate them. As synthesized by *Allen et al.* [2011], three principal kinematic roles have been suggested for the eastern Iranian faults, which are not mutually exclusive.

Table 6. (continued)

	Block Rotation Model Predictions				
Block Name	Total Rotation Inferred From Long-Term S_L (deg)	Long-Term Rotation Rate Inferred From Long-Term S_L (°/Ma)	Holocene Rotation Rate Inferred From Holocene Slip Rate S_H (°/Ma)	Current Rotation Rate Inferred From GPS Slip Rate S_C (°/Ma)	Current Westward and Eastward Velocities of Northern and Southern Tips of Rotating Faults Inferred From GPS Data (mm/yr)
CIB	22	1.5 ± 0.4	0.75 ± 0.5	0.4 ± 0.3	1.5
ADB	> 11.3	0.8 ± 0.2	> 0.3	0.75 ± 0.25	2
KAB	> 8	0.6 ± 0.1	~ 0.6	1.4 ± 0.5	3
NB	*>> 4*	*>> 0.2–0.3*	1.1 ± 0.2	1.3 ± 0.1	7.5
LB	17.6	1.2 ± 0.3	1.5 ± 0.8	1.1 ± 0.1	7.5
		1.0 ± 0.4	**1.0 ± 0.4**	**1.0 ± 0.4**	

The first possible role of the eastern Iranian faults is to permit the Iranian crust to move northward with respect to the stable Afghan crust at the eastern boundary of the collision zone [e.g., *Meyer et al*., 2006; *Masson et al*., 2007]. We show here that such a northward motion does occur and is accommodated by slip on the major ~ NS striking eastern Iranian faults. The faults cut the Iranian crust into five major crustal slivers, and those crustal blocks are currently moving northward at 6 to 13 mm/yr while the Afghan crust is stable. Their northward progression is driven by significant synthetic lateral slip on the major faults, especially on the three easternmost faults EL, WL, and KB. It is noteworthy that the northward velocity that we measure for the westernmost CIB, ADB, and KAB units (~ 13 mm/yr) is similar to the northward velocity estimated by *Regard et al*. [2005] for the Hormuz promontory due south of those units. This may suggest, as proposed by *Allen et al*. [2011], that the collective behavior of the ~ NS faults contributes to allow the Arabian promontory to impinge northward into the Eurasian crust.

Another possible role suggested for the eastern Iranian faults, at least for those having an obliquity with the convergence vector, is to accommodate the lateral component of slip, so that the rest of the slip, purely compressional, might be absorbed in NW trending thrust and fold systems (i.e., slip partitioning). Yet we note that our fault mapping, as for most available fault maps in eastern Iran, does not show much parallel NW trending strike-slip and reverse faults, as would be expected from this model. Rather, most of the NW trending thrust faults and folds that are observed in eastern Iran have developed at the tips of the major NS faults, in mechanical response to their right-lateral slip. Slip partitioning therefore seems to be limited in eastern Iran.

Finally, a third possible role that has long been suggested for the NS eastern Iranian faults is to achieve NS shortening by rotating counterclockwise in the horizontal plane [e.g., *Jackson and McKenzie*, 1984; *Walker et al*., 2004; *Walker and Jackson*, 2004; *Walker and Khatib*, 2006; *Allen et al*., 2011] (Figure 6). The rotation would provide a plane-strain way of taking up across zone shortening by NS reduction of the crustal width and EW elongation of the rotating zone. This mechanism requires, however, that the faults strike with some obliquity to the convergence vector.

Our GPS data show for the first time that the crustal slivers which the NS faults bound in eastern Iran are indeed currently rotating counterclockwise, at significant rates in the range 0.1–0.8°/Ma. We thus may use the GPS data to quantitatively test the rotation model. Moreover, by combining the GPS data with the information available on Holocene and longer-term fault movements, we may test the model over different time scales. We perform those tests below.

7.2.2. Vertical Axis Block Rotations in Eastern Iran

First, it is important to note that the ~ NS faults have strikes that rotate counterclockwise from ~ N10°E in the east (EL) to ~ N160°E in the west (DS fault), so that the faults resemble a fan anchored due north of the Hormuz promontory. The Lut faults, in continuity with this promontory, strike almost parallel to the plate convergence vector at that longitude (~ N13°E [*Masson et al*., 2007]). This suggests that the ~ NS faults of eastern Iran might have formed originally in a N-NNE direction, then rotated counterclockwise by amounts increasing westward from ~10° in the east to ~ 30° in the west. Recent paleomagnetic data provide support for this suggestion [*Mattei et al*., 2012]. The development of the faults in the prolongation of the Hormuz promontory might have been induced by the northward impingement of the Hormuz promontory into the Iranian crust, as observed in similar contexts in the world [e.g., *Tapponnier and Molnar*, 1976], and favored by the existence of inherited NS faults and sutures in this area [e.g., *Walker and Khatib*, 2006; *Cifelli et al*., 2013; *Nozaem et al*., 2013].

Vertical axis block rotations have been documented in many places in the world and shown to be an efficient mechanism to accommodate and to transfer strain (Figure 6 modified from *Manighetti et al*. [2001])

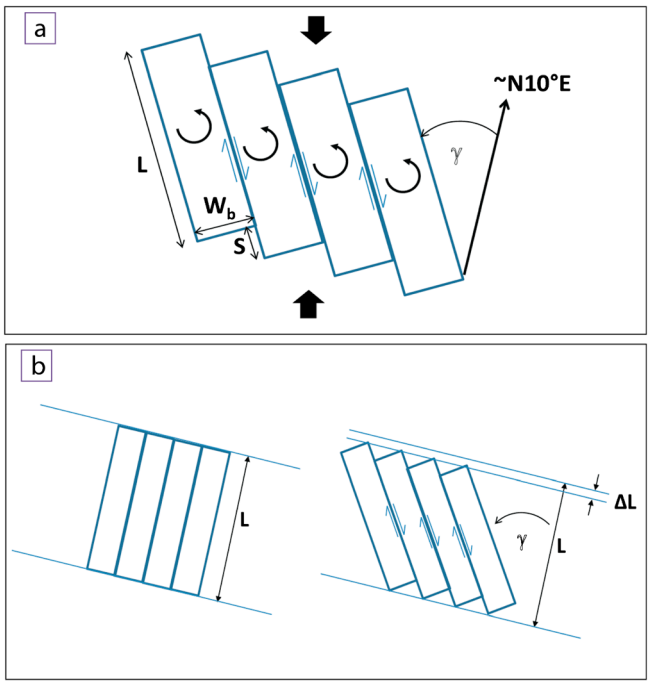

Figure 6. (a) Schematic representation of the vertical axis block rotation model under NS compression. The blocks have a length *L* and a width W_b. The rotation γ implies right-lateral slip (by a total amount *S*) on the faults bounding the blocks. (b) As blocks and faults are rotated, a width decrease (ΔL) in the total width of the rotating zone is induced [modified from *Manighetti et al.*, 2001]. This decrease may contribute to the progressive southward displacement of the fault traces north of the rotating zone, especially the Doruneh fault trace.

[e.g., *Freund*, 1970, 1974; *Macdonald et al.*, 1984; *Ron et al.*, 1984, 1986; *McKenzie and Jackson*, 1986; *Nur et al.*, 1986; *Mandl*, 1987; *Kleinrock and Hey*, 1989; *Tapponnier et al.*, 1990; *Acton et al.*, 1991; *Phipps Morgan and Kleinrock*, 1991; *Wetzel et al.*, 1993; *Martinez et al.*, 1997; *Manighetti et al.*, 2001]. The mechanism operates in a similar way regardless of the scale [*Manighetti et al.*, 2001]. It implies the rotation about a vertical axis of a limited number of rigid blocks bounded by subparallel synthetic strike-slip faults. Generally, the block rotation is driven by oblique stress acting on the edges or on the tips of the rotating blocks [e.g., *Freund*, 1970, 1974; *Ron et al.*, 1984, 1986; *Jackson and McKenzie*, 1984; *Nur et al.*, 1986].

Below we use the available data on total, Holocene and current deformation to examine whether they agree with the vertical axis block rotation model suggested by the GPS measurements. All these data are gathered in Table 6. They include the geometrical characteristics of the eastern Iranian blocks and faults that we estimated from our tectonic maps (fault lengths, block widths; Figures 1 and 2), the times of fault initiation inferred from literature, the cumulative maximum slips known on the faults, the late Quaternary, generally Holocene, slip rates available in the literature, and the current fault slip rates and block rotation rates that we estimated from the GPS data. If the blocks and faults have rotated counterclockwise by an angle γ, the right-lateral slip (*S*) resulting on each bounding fault depends on the width of the rotating block (W_b), such as $S = W_b \times \tan \gamma$ (Figure 6). We can thus use *S* to infer γ. Using the available data to perform the above calculations, we estimate that the CIB, ADB, KAB, and LB blocks have rotated counterclockwise by about 22, >11, >8, and 18° since 12–20 Ma (Table 6). NB is indicated in Table 6 for completeness but lacking constraints. These rotation amounts are in fair agreement with those previously inferred from the fault strikes and from paleomagnetic data [*Mattei et al.*, 2012]. The rotations occurred at moderate rates, of the order of 0.6–1.5°/Ma and averaging 1.0 ± 0.4°/Ma (Table 6). The Holocene and current fault slip rates can also be used to estimate the Holocene and current rotation rates. Those are found to be on the same order than the long-term rotation rates, with similar values of 0.3–1.5°/Ma (Holocene) and 0.4–1.4°/Ma (current) over the five blocks (Table 6). The average rotation rates are the same over the three periods of time, 1.0 ± 0.4°/Ma (Table 6). The rotation rates inferred from the block rotation model, including the current rates, are similar within uncertainties to those that we measured in the GPS data (0.4 ± 0.25°/Ma). This suggests that the vertical axis block rotation model satisfactorily describes the kinematics of the ~NS eastern Iranian faults.

The next question is to understand why the ~NS faults and blocks have been led to rotate in the horizontal plane. Over "recent times" (i.e., likely few last Ma up to present), the obliquity of most of the (already rotated) ~NS faults with respect to the convergence vector easily accounts for the origin of the lateral shear that drives the rotations (Figure 6). In contrast, if the faults formed initially with a strike primarily parallel to the convergence vector, they were not sustaining any lateral stress and hence had no reason, originally, to start rotating. The block rotation model allows the calculation of the block-perpendicular, lateral shear (V_{sh}) that might be needed to make the blocks rotate ($\gamma = \arctan(2V_{sh} \times T/L)$, with γ the total rotation, L the length of the rotating blocks, and T the duration of the rotation) [e.g., *Tapponnier et al*., 1990; *Manighetti et al*., 2001]. The shear V_{sh} can thus be expressed as $V_{sh} = (S \times L)/2(T \times W_b)$. The long-term, Holocene and current fault slips and slip rates (Table 6) can be used to estimate V_{sh} (considered here on each side of the rotating zone). We find that V_{sh} is in a similar range in the three periods of time, 3–7 mm/yr. At the time that the ~NS faults were formed, the two parallel, overlapping, NW trending Kopeh Dagh and Main Recent faults were slipping right-laterally at 7–16 mm/yr [*Lyberis and Manby*, 1999; *Allen et al*., 2004; *Shabanian et al*., 2009a] and 10–15 mm/yr (at least west of ~52°E) [*Talebian and Jackson*, 2002; *Bachmanov et al*., 2004], respectively. We hypothesize that the coeval right-lateral motions on those two overlapping faults might have induced ~E-W lateral shear at the tips of the ~NS faults and blocks enclosed between their traces, which forced them to start rotating counterclockwise, away from their original NNE strike.

The block rotation model is necessarily a simplification of the actual processes. In particular, the blocks have slightly different sizes and thus, rotation rates, and those differences might induce extensional or compressional deformation across the faults as the rotating blocks indent or separate from each other. This observation is in keeping with the small across-strike fault motions found in the GPS data.

The vertical axis block rotation model also allows the calculation of the westward and eastward velocities of the northern and southern tips, respectively, of the rotating faults (calculations in Figure S5 and Table 6). Those velocities are calculated with respect to the center of each fault, which has a null EW velocity. The EW velocity gradients along the rotating faults are thus an indicator of the strain that is accumulating at the tips of the rotating faults and blocks. From GPS fault slip rates and block dimensions we find that the fault tips are moving currently at significant EW velocities, averaging 1–2 mm/yr for the Dehshir and Anar fault tips, 3 mm/yr for the Kuhbanan fault tips, and 7–8 mm/yr for the WL and EL fault tips. Since those velocities are inferred from simple calculations, they should be considered with caution. However, they suggest that significant strain occurs at the tips of the rotating faults, where they might produce deformation, as suggested in prior works [e.g., *Freund*, 1970, 1974; *Ron et al*., 1984, 1986; *Nur et al*., 1986; *Manighetti et al*., 2001; *Walker and Jackson*, 2004]. Dense, distributed, secondary faulting is expected to develop at the rotating tips and to be mainly compressional in the NW and SE tip quadrants of the faults, while being mainly extensional in their NE and SW tip quadrants. These expectations are consistent with the observed development of dense secondary thrust fault networks at the NW and SE tips of all northerly striking eastern Iranian faults, especially the west and east Lut faults. The tip velocities that we infer from the rotating block model suggest that secondary faulting might be most developed and most active at the tips of the EL and WL faults, significant at the tips of the KB fault, and more moderate at the tips of the Anar and Dehshir faults. Figure 1 shows that the fault tips that we infer as being most active are those showing the densest and largest seismic activity. In contrast, the fault tips that we infer as sustaining lower strain are those free of earthquakes. Together, these suggest that a significant part of the earthquake activity in eastern Iran might result from the secondary faults at the tips of the rotating master faults breaking to release the large strain and stress that they sustain due to the rotation of the master faults.

7.2.3. The Specific Role of the Doruneh Fault

Prior studies have suggested that the Doruneh fault and possibly also nearby ~EW faults might sustain vertical axis clockwise rotations in the horizontal plane [*Jackson and McKenzie*, 1984; *Walker et al*., 2004; *Walker and Jackson*, 2004; *Allen et al*., 2006; *Walker and Khatib*, 2006; *Hollingsworth et al*., 2010]. No data were available however to test this hypothesis. The rotations were proposed to result from the eastward increase in the right-lateral slip rates of the eastern ~NS Iranian faults. Yet as pointed out by *Farbod et al*. [2011], the mechanical reasons for those supposed clockwise rotations along the entire length of the Doruneh fault are not clear, whereas the present strike and geometry of the Doruneh fault are difficult to conciliate with the supposed clockwise rotations. Furthermore, recent paleomagnetic data show no significant clockwise rotation over the Neogene along the Doruneh fault [*Mattei et al*., 2012]. The GPS data suggest a 0.7–0.8°/Ma clockwise rotation in the Doruneh area. The rotation is constrained, however, by GPS stations spread over

large distances that certainly exceed the limits of a rigid unit. Therefore, the available data cannot be used to test the models that have been proposed so far. Additional data and possibly further thoughts are needed to understand how the Doruneh and nearby ~ EW faults collectively accommodate part of the NS convergence.

While the GPS data do not allow the discussion of the mechanical reasons for the formation of the Doruneh fault, almost perpendicular to most major faults in eastern Iran, the vertical axis block rotation model that we propose provides suggestions. We speculate that the curved shape of the Doruneh fault trace might result from the block rotations occurring further south. The fault might have been forced to "follow" the overall southwestward displacement of the rotating ~ NS blocks ("space opening" or reduction of the region width, because of the rotations; Figure 6b) [*Manighetti et al*., 2001]. This "southwestward attraction" might have contributed to curve the overall fault trace. The curving might have occurred through the southward jump of the principal fault segments, identified by *Farbod et al*. [2011]. The southwestward "pulling" of the fault trace might force the fault to propagate southwestward. If the Doruneh fault does propagate toward the SW, we may anticipate that it might eventually connect with the Main Recent fault. Should such a connection occur, the vertical axis block rotations in eastern Iran would be likely to stop.

8. Conclusions

We have analyzed new, dense, 11 year long GPS data (92 stations) that we acquired in eastern Iran in the framework of the long-lasting Iranian-French collaboration. The density and quality of the GPS data, combined with our detailed analysis of the seismogenic faults that accommodate the current strain, have allowed us to estimate, for the first time, the present-day kinematics and the slip rates on most faults in eastern Iran. The current kinematics is fairly well described by a rigid block model although a number of secondary faults exist which complicate this scenario. We confirm that the east Lut, west Lut, Kuhbanan, Anar, Dehshir, and Doruneh faults are the major and fastest-slipping faults in eastern Iran, and we show that those faults are currently slipping laterally at 5.6 ± 0.6, 4.4 ± 0.4, 3.6 ± 1.3, 2.0 ± 0.7, 1.4 ± 0.9, and 1.3 ± 0.8 mm/yr, respectively. The slip is right-lateral on all five N-NNW striking faults (EL, WL, KB, A, DS), while it is left-lateral on the Doruneh fault. The N-NNW faults bound fairly rigid blocks that move in the N13°E ARA-EUR convergence direction at fast rates with respect to Eurasia, ranging between ~ 1 and 13 mm/yr from east to west. The blocks also move toward the WNW at rates between 1 and 5 mm/yr from east to west (with respect to Eurasia), and each rotates counterclockwise in the horizontal plane at rates ranging from 0.1 to 0.8°/Ma. The current fault slip rates are roughly similar to the long-term and Holocene slip rates provided in the literature. A vertical axis block rotation model well describes the current kinematics in eastern Iran. Available data on longer-term fault motions are also well reproduced with the model, which suggests that the counterclockwise rotations might have been operating at a similar rate since at least 12 Ma.

Therefore, the GPS data suggest that the northward convergence is accommodated in eastern Iran in two ways. First, the eastern Iranian crust is sliced into five large ~ NS trending slivers, and those crustal slivers are moving northward at fast rates (6–13 mm/yr) with respect to the stable Afghan crust at the eastern edge of the collision zone. It is likely that the collective behavior of the ~ NS faults contributes to allow the Arabian promontory to impinge northward into the Eurasian crust. Second, the ~ NS eastern Iranian faults achieve NS shortening by rotating counterclockwise in the horizontal plane. The rotation has been occurring over the last 12–20 Ma up to present, at a similar rate averaging 1 ± 0.4°/Ma. The vertical axis block rotation mechanism provides a plane-strain way of taking up across zone shortening by NS reduction of the crustal width and EW elongation of the rotating zone. We believe that the dynamics of the motions is dominantly controlled by the compressive forces at the Zagros and Makran collision zones and a more localized force being applied at the Hormuz indenter. Yet there is still the possibility that the internal buoyancy forces also play a secondary role, as suggested in Asia [e.g., *Vilotte et al*., 1986; *Houseman and England*, 1993].

Our work has implications on the understanding of part of the earthquake activity in eastern Iran. We expect that, over the several million years of block rotations, long-term diffuse and complex secondary faulting was created at the rotating fault tips. Such secondary faulting is, in fact, observed. We used the GPS data to estimate the westward and eastward velocities of the rotating fault tips. We found those velocities especially elevated at the tips of the EL, WL, and KB rotating faults, exactly where historical and

instrumental earthquake activity is remarkably localized and prevalent. We thus suggest that particular attention should be paid to the major fault tips, as those zones are the locus of elevated stresses and strain induced by the counterclockwise rotations. GPS data would also be needed in those zones to accurately measure the strain which accumulates there, in preparation for forthcoming earthquakes. We suggest that the Dasht-e-Bayaz, Sedeh, and Birjand faults might have formed recently to contribute to the westward displacement of the east Lut rotating fault trace, whereas the Doruneh fault might have its trace forced to migrate southwestward as the ~NS blocks rotate counterclockwise. It has been shown that young, immature faults produce higher stress drop earthquakes than long-lived faults [*Manighetti et al.*, 2007]. The presumed immaturity of the Dasht-e-Bayaz fault might explain why, despite the fault having a low slip rate, it broke in two large, high stress drop earthquakes within a very short time interval (1968 and 1979). We suggest that a similar behavior might be expected on the Sedeh and Birjand faults due south of Dasht-e-Bayaz, and possibly on the western half of the Doruneh fault. Special attention should thus be paid to those faults, as they could be the locus of forthcoming large earthquakes.

Acknowledgments

We thank the National Cartographic Center in Tehran for the precious help in conducting the field measurements presented in our work, in particular, NCC head M. Ilkhan and H. Vaezi. We are also very grateful to the members of the geodynamic department for the management of the permanent GPS data, with particular thanks to Z. Rahimi. Thanks to the many NCC members who participated in the field work, organized perfectly by H. Hendi, A. Rahmani, M. Sardari, and A. Nemati. F. Tavakoli's PhD thesis grant has been provided by TOTAL. The French Embassy in Tehran helped funding the research trainings of Z. Mousavi, A. Jadidi, A. Aghamohammadi, and H. Nankali. French participants in the field work have been supported by the INSU-CNRS project Dyeti. Particular thanks to S. Baize and C. Sue for their help in the field reconnaissance. We are grateful to Y. Gaudemer for the thorough discussions that we had. W. Hammond and W. Thatcher greatly improved the present manuscript by their very constructive reviews. Many thanks to F. Lodge for helping us with the English writing adjustments.

References

Acton G. D., S. Stein, and J. F. Engelen (1991), Block rotation and continental extension in Afar: A comparison to oceanic microplate system, *Tectonics*, *10*, 501-526.

Allen, M. B., C. Saville, E. Blanc, M. Talebian, and E. Nissen (2013), Orogenic plateau growth: Expansion of the Turkish-Iranian Plateau across the Zagros fold and thrust belt, *Tectonics*, *32*, 171-190, doi:10.1002/tect.20025.

Allen, M. B., J. Jackson, and R. T. Walker (2004), Late Cenozoic reorganization of the Arabia-Eurasia collision and the comparison of short-term and long-term deformation rates, *Tectonics*, *23*, TC2008, doi:10.1029/2003TC001530.

Allen, M. B., E. J.-P. Blanc, R. T. Walker, J. Jackson, M. Talebian, and M. R. Ghassemi (2006), Contrasting styles of convergence in the Arabia-Eurasia collision: Why escape tectonics does not occur in Iran, *GSA Special Pap.*, *409*, 579-589, doi:10.1130/2006.2409(26).

Allen, M. B., M. Kheirkhah, M. H. Emami, and S. J. Jones (2011), Right-lateral shear across Iran and kinematic change in the Arabia–Eurasia collision zone, *Geophys. J. Int.*, *184*, 555–574.

Ambraseys, N. N., and C. Melville (1982), *A History of Persian Earthquakes*, 240 pp., Cambridge Univ. Press, Cambridge, U. K.

Ambraseys, N. N., and J. S. Tchalenko (1969), The Dasht-e-Bayaz (Iran) earthquake of August 31, 1968: A field report, *Bull. Seismol. Soc. Am.*, *59*, 1751 – 1792.

Bachmanov, D. M., V. G. Trifonov, K. T. Hessami, A. I. Kozhurin, T. P. Ivanova, E. A. Rogozhin, M. C. Hademi, and F. H. Jamali (2004), Active faults in the Zagros and central Iran, *Tectonophysics*, *380*, 221–241.

Bayer, R., J. Chéry, M. Tatar, P. Vernant, M. Abbassi, F. Masson, F. Nilforoushan, E. Doerflinger, V. Regard, and O. Bellier (2006), Active deformation in Zagros-Makran transition zone inferred from GPS measurements, *Geophys. J. Int.*, *165*,173–181.

Bellier, O., S. Över, A. Poisson, and J. Andrieux (1997), Recent temporal change in the stress state and modern stress field along the North Anatolian Fault Zone (Turkey), *Geophys. J. Int.*, *131*, 61–86.

Berberian, M. (1976), Contribution to the seismotectonics of Iran (Part II), *Ministry of Industry and Mines, Geological Survey of Iran, Tectonic and Seismotectonic Section (Tehran)*.

Berberian, M. (1981), Active faulting and tectonics of Iran, in *Zagros-Hindu Kush-Himalaya Geodynamic Evolution*, Geodynamics Series, vol. 3, edited by H. K. Gupta and F. M. Delany, pp. 33–69, AGU, Washington, D. C.

Berberian, M., and M. Qorashi (1994), Coseismic fault-related folding during the South Golbaf earthquake of November 20, 1989, in southeast Iran, *Geology*, *22*(6), 531–534.

Berberian, M., and R. S. Yeats (1999), Patterns of historical earthquake rupture in the Iranian Plateau, *Bull. Seismol. Soc. Am. 89*, 120–139.

Berberian, M., I. Asudeh, and S. Arshadi (1979), Surface rupture and mechanism of the Bob-Tangol (southeastern Iran) earthquake of December 19, 1977, *Earth Planet. Sci. Lett.*, *42*(3), 456–462.

Berberian, M., J. A. Jackson, M. Qorashi, M. M. Khatib, K. Priestley, M. Talebian, and M. Ghafuri-Ashtiani (1999), The 1997 May 10 Zirkuh (Qaenat) earthquake (*Mw* 7.2): Faulting along the Sistan suture zone of eastern Iran, *Geophys. J. Int.*, *136*, 671–694.

Berberian, M., J. A. Jackson, M. Qorashi, M. Talebian, M. Khatib, and K. Priestley (2000), The 1994 Sefidabeh earthquakes in eastern Iran: Blind thrusting and bedding-plane slip on a growing anticline, and active tectonics of the Sistan suture zone, *Geophys. J. Int.*, *142*(2), 283–299.

Berberian, M., J. A. Jackson, E. Fielding, B. E. Parsons, K. Priestley, M. Qorashi, M. Talebian, R. T. Walker, T. J. Wright, and C. Baker (2001), The 1998 March 14 Fandoqa earthquake (*Mw* 6.6) in Kerman province, southeast Iran: Re-rupture of the 1981 Sirch earthquake fault, triggering of slip on adjacent thrusts and the active tectonics of the Gowk fault zone, *Geophys. J. Int.*, *146*, 371–398, doi:10.1046/j.1365-246x.2001.01459.x.

Cifelli, F., M. Mattei, H. Rashid, and J. Ghalamghash (2013), Right-lateral transpressional tectonics along the boundary between Lut and Tabas blocks (Central Iran), *Geophys. J. Int.*, *193*(3), 1153–1165.

Djamour, Y., et al. (2010), GPS and gravity constraints on continental deformation in the Alborz mountain range, Iran, *Geophys. J. Int.*, *183*, 1287–1301.

Dow, J. M., R. E. Neilan, and C. Rizos (2009), The International GNSS Service in a changing landscape of Global Navigation Satellite Systems, *J. Geodesy*, *83*, 191–198.

Engdahl, E. R., and A. Villaseñor (2002), 41 global seismicity: 1900–1999, *Int. Geophys.*, *81*, 665–XVI.

Engdahl, E. R., J. A. Jackson, S. Myers, E. Bergman, and K. Priestley (2006), Relocation and assessment of seismicity in the Iran region, *Geophy. J. Int.*, *167*, 761–788.

Farbod, Y., O. Bellier, E. Shabanian, and M. R. Abbassi (2011), Geomorphic and structural variations along the Doruneh Fault System (central Iran), *Tectonics*, *30*, TC6014, doi:10.1029/2011TC002889.

Fattahi, M., R. T. Walker, M. M. Khatib, A. Dolati, and A. Bahroudi (2007), Slip-rate estimate and past earthquakes on the Doruneh fault, eastern Iran, *Geophys. J. Int.*, *168*, 691–709, doi:10.1111/j.1365-246X.2006.03248.x.

Fattahi, M., H. Nazari, M. D. Bateman, B. Meyer, M. Sébrier, M. Talebian, K. Le Dortz, M. Foroutan, F. Ahmadi Givi, and M. Ghorashi (2010), Refining the OSL age of the last earthquake on the Dehshir fault, Central Iran, *Quat. Geochronology*, *5*, 2–3, 286–292, doi:10.1016/j.quageo.2009.04.005.

Foroutan, M., M. J. Bolourchi, S. Solaymani Azad, B. Oveisi, M. Nemati, M. A. Shokri, and M. Eskandari (2010), Primary report of Konarak earthquake 2010 Dec 20 (Rigan, Kerman), Online Report, Geological Survey of Iran. [http://www.gsi.ir/Science.html.]

Freund, R. (1970), Rotation of strike slip faults in Sistan, southeast Iran, *J. Geol.*, 188–200.
Freund, R. (1974), Kinematics of transform and transcurrent faults, *Tectonophysics*, *21*(1), 93–134.
Herring, T. A., R. W. King, and S. C. McClusky (2006), Introduction to GAMIT/GLOBK, Release 10.3, *Dep. of Earth Atmos. and Planet. Sci., Mass. Inst. of Technol., Cambridge, Mass*.
Hollingsworth, J., J. A. Jackson, R. T. Walker, M. Gheitanchi, and M. Bolourchi (2006), Strike-slip faulting, rotation, and along-strike elongation in the Kopeh Dagh mountains, NE Iran, *Geophy. J. Int.*, *166*, 1161–1177.
Hollingsworth, J., J. A. Jackson, R. T. Walker, and H. Nazari (2008), Extrusion tectonics and subduction in the eastern South Caspian region since 10 Ma, *Geology*, *36*(10), 763–766.
Hollingsworth, J., M. Fattahi, R. T. Walker, M. Talebian, A. Bahroudi, M. Bolourchi, J. A. Jackson, and A. Copley (2010a), Oroclinal bending, distributed thrust and strike-slip faulting, and the accommodation of Arabia-Eurasia convergence in NE Iran since the Oligocene, *Geophys. J. Int.*, *181*, 1214–1246.
Hollingsworth, J., H. Nazari, J.-F. Ritz, R. Salamati, M. Talebian, M. Bahroudi, R. T. Walker, M. Rizza, and J. Jackson (2010b), Active tectonics of the east Alborz mountains, NE Iran: Rupture of the left-lateral Astaneh fault system during the great 856 A.D. Qumis earthquake, *J. Geophys. Res.*, *115*, B12313, doi:10.1029/2009JB007185.
Houseman, G., and P. England (1993), Crustal thickening versus lateral expulsion in the Indian-Asian continental collision, *J. Geophys. Res.*, *98*(B7), 12,233–12,249.
Jackson, J., and D. McKenzie (1984), Active tectonics of the Alpine-Himalayan belt between Turkey and Pakistan, *Geophys. J. Int. 77*(1), 185–264.
Jackson, J. A., A. J. Haines, and W. E. Holt (1995), The accommodation of Arabia–Eurasia plate convergence in Iran, *J. Geophys. Res.*, *100*, 15,205–15,219.
Javidfakhr, B., O. Bellier, E. Shabanian, L. Siame, L. Léanni, D. Bourlès, and S. Ahmadian (2011), Fault kinematics and active tectonics at the southeastern boundary of the eastern Alborz (Abr and Khij fault zones): Geodynamic implications for NNE Iran, *J. Geodyn.*, *52*(3), 290–303.
Kleinrock, M. C., and R. N. Hey (1989), Migrating transform zone and lithospheric transfer at the Galapagos 95.5°W propagator, *J. Geophys. Res.*, *94*, 13,859–13,878.
Le Dortz, K., et al. (2009), Holocene right-slip rate determined by cosmogenic and OSL dating on the Anar fault, central Iran, *Geophys. J. Int.*, *179*(2), 700–710, doi:10.1111/j.1365-246X.2009.04309.x.
Le Dortz, K., et al. (2011), Dating inset terraces and offset fans along the Dehshir Fault (Iran) combining cosmogenic and OSL methods, *Geophys. J. Int.*, *185*(3), 1147–1174.
Lyberis, N., and G. Manby (1999), Oblique to orthogonal convergence across the Turan block in the post-Miocene, *AAPG Bull.*, *83*(7), 1135–1160.
Macdonald, K. C., J. C. Sempere, and P. J. Fox (1984), East Pacific Rise from Sioqueiros to Orozco fracture zones: Structure and evolution of overlapping spreading centers, *J. Geophys. Res.*, *89*, 6301–6306.
Maggi, A., J. A. Jackson, K. Priestley, and C. Baker (2000), A re-assessment of focal depth distributions in Southern Iran, the Tien Shan and Northern India: Do earthquakes really occur in the continental mantle, *Geophys. J. Int.*, *143*, 629–661.
Mandl, G. (1987), Tectonic deformation by rotating parallel faults: The "bookshelf" mechanism, *Tectonophysics*, *141*, 227–316.
Manighetti I., P. Tapponnier, V. Courtillot, Y. Gallet, E. Jacques, and P. Y. Gillot (2001), Strain transfer between disconnected, propagating rifts in Afar, *J. Geophys. Res. 106*, 13,613–13,665.
Manighetti, I., M. Campillo, S. Bouley, and F. Cotton (2007), Earthquake scaling, fault segmentation, and structural maturity, *Earth Planet. Sci. Lett.*, *253*(3–4), 429–438.
Manighetti, I., D. Zigone, M. Campillo, and F. Cotton (2009), Self-similarity of the largest-scale segmentation of the faults; implications on earthquake behavior, *Earth Planet. Sci. Lett.*, *288*, 370–381.
Manighetti, I., L. De Barros, C. Caulet, C. Perrin, and F. Cappa (2013), Deterministic, self-similar slip and stress heterogeneity on seismogenic faults, AGU San Francisco, Dec. 2013.
Martinez, F., R. N. Hey, and P. D. Johnson (1997), The east ridge system 28.5-32°S East Pacific Rise: Implications for overlapping spreading center development, *Earth Planet. Sci. Lett.*, *151*, 13–31.
Masson, F., J. Chéry, J. Martinod, D. Hatzfeld, P. Vernant, F. Tavakoli, and A. Ashtiani (2005), Seismic versus aseismic deformation in Iran inferred from GPS and seismicity data, *Geophys. J. Int.*, *160*, 217–226.
Masson, F., M. Anvari, Y. Djamour, A. Walpersdorf, F. Tavakoli, M. Daignières, H. Nankali, and S. van Gorp (2007), Large-scale velocity field and strain tensor in Iran inferred from GPS measurements: New insight for the present-day deformation pattern within NE Iran, *Geophys. J. Int.*, *170*, 436–440.
Mattei, M., F. Cifelli, G. Muttoni, A. Zanchi, F. Berra, F. Mossavvari, and S. A. Eshraghi (2012), Neogene block rotation in central Iran: Evidence from paleomagnetic data, *Geol. Soc. Am. Bull.*, *124*(5–6), 943–956.
McCaffrey, R., M. D. Long, C. Goldfinger, P. Zwick, J. Nabelek, and C. Smith (2000), Rotation and plate locking at the southern Cascadia subduction zone, *Geophy. Res. Lett.*, *27*, 3117–3120.
McCalpin, J. P., and A. R. Nelson (1996), Introduction to paleoseismology, *Int. Geophys.*, *62*, 1–32.
McClusky, S., R. Reilinger, S. Mahmoud, D. Ben Sari, and A. Tealeb (2003), GPS constraints on Africa (Nubia) and Arabia plate motions, *Geophys. J. Int.*, *155*(1), 126–138.
McKenzie, D. P., and J. A. Jackson (1986), A block model of distributed deformation by faulting, *J. Geol. Soc. London*, *143*, 349–353
Meyer, B., and K. Le Dortz (2007), Strike-slip kinematics in Central and eastern Iran: Estimating fault slip-rates averaged over the Holocene, *Tectonics*, *26*, TC5009, doi:10.1029/2006TC002073.
Meyer, B., F. Mouthereau, O. Lacombe, and P. Agard (2006), Evidence of Quaternary activity along the Deshir Fault: Implication for the Tertiary tectonics of Central Iran, *Geophys. J. Int.*, *164*, 192–201.
Mooney, W. D., G. Laske, and G. Masters (1998), CRUST-5.1: A global crustal model at 5 × 5 degrees, *J. Geophys. Res.*, *103*, 727–747.
Mousavi, Z., A. Walpersdorf, R. T. Walker, F. Tavakoli, E. Pathier, H. Nankali, F. Nilfouroushan, and Y. Djamour (2013), Global Positioning System constraints on the active tectonics of NE Iran and the South Caspian region, *Earth Planet. Sci. Lett.*, *377–378*, 287–298.
Nazari, H., M. Fattahi, B. Meyer, M. Sebrier, M. Talebian, M. Foroutan, K. Le Dortz, M. Bateman, and M. Ghorashi (2009), First evidence for large earthquakes on the Deshir fault, central Iran Plateau, *Terra Nova*, *21*(6), 417–426.
Nilforoushan, F., et al. (2003), GPS network monitors the Arabia–Eurasia collision deformation in Iran, *J. Geodesy 77*, 411–422.
Nowroozi, A. A., and A. Mohajer-Ashjai (1985), Fault movements and tectonics of the eastern Iran: Boundaries of the Lut plate, *Geophys. J. R. Astron. Soc.*, *83*, 215–237.
Nozaem, R., M. Mohajjel, F. Rossetti, M. Della Seta, G. Vignaroli, A. Yassaghi, F. Salvini, and M. Eliassi (2013), Post-Neogene right-lateral strike–slip tectonics at the north-western edge of the Lut Block (Kuh-e–Sarhangi Fault), Central Iran, *Tectonophysics*, *589*, 220–233.
Nur, A., H. Ron, and O. Scotti (1986), Fault mechanics and the kinematics of block rotation, *Geology*, *14*,746–749.

Parsons, B., T. Wright, P. Rowe, J. Andrews, J. A. Jackson, R. T. Walker, M. Khatib, M. Talebian, E. Bergman, and E. R. Engdahl (2006), The 1994 Sefidabeh (eastern Iran) earthquakes revisited: New evidence from satellite radar interferometry and carbonate dating about the growth of an active fold above a blind thrust fault, *Geophys. J. Int.*, *164*, 202–217, doi:10.1111/j.1365-246X.2005.02655.x.

Phipps Morgan, J., and M. C. Kleinrock (1991), Transform zone migration: Implications of bookshelf faulting at oceanic and icelandic propagation ridges, *Tectonics*, *10*, 920–935

Regard, V., et al. (2005), Cumulative right-lateral fault slip rate across the Zagros–Makran transfer zone: Role of the Minab–Zendan fault system in accommodating Arabia–Eurasia convergence in southeast Iran, *Geophys. J. Int.*, *162*(1), 177–203.

Reilinger, R., et al. (2006), GPS constraints on continental deformation in the Africa-Arabia-Eurasia continental collision zone and implications for the dynamics of plate interactions, *J. Geophys. Res.*, *111*, B05411, doi:10.1029/2005JB004051.

Ron, H., R. Freund, Z. Garfunkel, and A. Nur (1984), Block rotation by strike-slip faulting: Structural and paleomagnetic evidence, *J. Geophys. Res.*, *89*(B7), 6256–6270.

Ron, H., A. Aydin, and A. Nur (1986), Strike-slip faulting and block rotation in the Lake Mead fault system, *Geology*, *14*(12), 1020–1023.

Savage, J., and R. Burford (1973), Geodetic determination of relative plate motion in Central California, *J. Geophys. Res.*, *78*(5), 832–845, doi:10.1029/JB078i005p00832.

Sella, G. F., T. H. Dixon, and A. Mao (2002), REVEL: A model for recent plate velocities from space geodesy, *J. Geophys. Res.*, *107*, 2081, doi:10.1029/2000JB000033.

Sengor, A. M. C. (1990), A new model for the late Palaeozoic-Mesozoic tectonic evolution of Iran and implications for Oman, in *The Geology and Tectonics of the Oman Region*, edited by A. H. F. Robertson, M. P. Searle, and A. C. Ries, *Geol. Soc. Spec. Publ.*, *49*, 797–831, London, U. K.

Sengor, A. M. C., and W. S. F. Kidd (1979), Postcollisional tectonics of the Turkish-Iranian plateau and a comparison with Tibet, *Tectonophysics*, *55*, 361–376.

Shabanian, E., L. Siame, O. Bellier, L. Benedetti, and M. R. Abbassi (2009a), Quaternary slip rates along the northeast boundary of the Arabia-Eurasia collision zone (Kopeh Dagh Mountains, north-east Iran), *Geophys. J. Int.*, *178*, 1055–1077.

Shabanian, E., O. Bellier, L. Siame, N. Arnaud, M. R. Abbassi, and J. J. Cocheme (2009b), New tectonic configuration in NE Iran: Active strike-slip faulting between the Kopeh Dagh and Binalud mountains, *Tectonics 28*, TC5002, doi:10.1029/2008TC002444.

Stocklin, J., and N. H. Nabavi (1972), *Tectonic Map of Iran*, Geol. Surv Iran, Tehran, Iran.

Talebian, M., and J. A. Jackson (2002), Offset on the Main Recent Fault of the NW Iran and implications on the late Cenozoic tectonics of the Arabia-Eurasia collision zone, *Geophys. J. Int.*, *150*, 422–439.

Talebian, M., et al. (2004), The 2003 Bam (Iran) earthquake: Rupture of a blind strike-slip fault, *Geophys. Res. Lett.*, *31*, L11611, doi:10.1029/2004GL020058.

Talebian, M., et al. (2006), The Dahuiyeh (Zarand) earthquake of 2005 February 22 in central Iran: Reactivation of an intramountain reverse fault. *Geophys. J. Int.*, *164*, 137–148, doi:10.1111/j.1365-246X.2005.02839.x.

Tapponnier, P., and P. Molnar (1976), Slip-line field theory and large scale continental tectonics, *Nature*, *264*, 319-324.

Tapponnier, P., R. Armijo, I. Manighetti, and V. Courtillot (1990), Bookshelf faulting and horizontal block rotations between overlapping rifts in southern Afar, *Geophys. Res. Lett.*, *17*, 1, 1–4.

Tatar, M., D. Hatzfeld, J. Martinod, A. Walpersdorf, M. Ghafori-Ashtiany, and J. Chery (2002), The present-day deformation of the central Zagros from GPS measurements, *Geophys. Res. Lett.*, *29*(19), 1927, doi:10.1029/2002GL015427.

Tavakoli, F. (2007), Present-day kinematics of the Zagros and east of Iran faults, PhD. thesis, Univ. of Joseph Fourier, Grenoble, France.

Tavakoli, F., A. Walpersdorf, C. Authemayou, H. R. Nankali, D. Hatzfeld, M. Tatar, Y. Djamour, F. Nilforoushan, and N. Cotte (2008), Distribution of the right-lateral strike-slip motion from the Main Recent Fault to the Kazerun Fault System (Zagros, Iran): Evidence from present-day GPS velocities, *Earth Planet. Sci. Lett.*, *275*(3), 342–347, doi:10.1016/j.epsl.2008.08.030.

Tchalenko, J. S., and M. Berberian (1975), Dasht-e-Bayaz fault, Iran: Earthquake and earlier related structures in bedrock, *Geol. Soc. Am. Bull.*, *86*, 703–709.

Vergnolle, M., A. Walpersdorf, V. Kostoglodov, P. Tregoning, J. A. Santiago, N. Cotte, and S. I. Franco (2010), Slow slip events in Mexico revised from the processing of 11-year GPS observations, *J. Geophys. Res.*, *115*, B08403, doi:10.1029/2009JB006852.

Vernant, P., et al. (2004a), Contemporary crustal deformation and plate kinematics in middle east constrained by GPS measurement in Iran and northern Oman, *Geophys. J. Int.*, *157*, 381–398.

Vernant, P., F. Nilforoushan, J. Chéry, R. Bayer, Y. Djamour, F. Masson, H. Nankali, J.-F. Ritz, M. Sedighi, and F. Tavakoli (2004b), Deciphering oblique shortening of central Alborz in Iran using geodetic data, *Earth Planet. Sci. Lett.*, *223*, 177–185.

Vilotte, J. P., R. Madariaga, M. Daignieres, and O. Zienkiewicz (1986), Numerical study of continental collision: Influence of buoyancy forces and an initial stiff inclusion. *Geophys. J. Roy. Astron. Soc.*, *84*(2), 279–310.

Walker, F., and M. B. Allen (2012), Offset rivers, drainage spacing and the record of strike-slip faulting: The Kuh Banan Fault, Iran, *Tectonophysics*, *530*, 251–263.

Walker, R. T., and M. M. Khatib (2006), Active faulting in the Birjand region of NE Iran. *Tectonics*, *25*, TC4016, doi:10.1029/2005TC001871.

Walker, R. T., E. A. Bergman, W. Szeliga, and E. J. Fielding (2011), Insights into the 1968–1997 Dasht-e-Bayaz and Zirkuh earthquake sequences, eastern Iran, from calibrated relocations, InSAR and high-resolution satellite imagery, *Geophys. J. Int.*, doi:10.1111/j.1365-246X.2011.05213.x

Walker, R. T. (2006), A remote sensing study of active folding and faulting in southern Kerman province, S.E. Iran, *J. Struct. Geol.*, *284*, 654–668. 10.1016/j.jsg.2005.12.014.

Walker, R. T., and J. A. Jackson (2002), Offset and evolution of the Gowk fault, SE Iran: A major intra-continental strike-slip system, *J. Struct. Geol.*, *24*, 1677–1698.

Walker, R. T., and J. A. Jackson (2004), Active tectonics and late Cenozoic strain distribution in central and eastern Iran. *Tectonics*, *23*, TC5010, doi:10.1029/2003TC001529.

Walker, R. T., J. A. Jackson, and C. Baker (2003), Surface expression of thrust faulting in eastern Iran: Source parameters and surface deformation of the 1978 Tabas and 1968 Ferdows earthquake sequences, *Geophys. J. Int.*, *152*, 749–765, doi:10.1046/j.1365-246X.2003.01886.x.

Walker, R. T., J. A. Jackson, and C. Baker (2004), Active faulting and seismicity of the Dasht-e-Bayaz region, eastern Iran, *Geophys. J. Int.*, *157*, 265–282.

Walker, R. T., P. Gans, M. B. Allen, J. A. Jackson, M. M. Khatib, N. Marsh, and M. Zarrinkoub (2009), Late Cenozoic volcanism and rates of active faulting in eastern Iran, *Geophys. J. Int.*, *177*, 783–805.

Walker, R. T., M. Talebian, R. A. Sloan, A. Rasheedi, M. Fattahi, and C. Bryant (2010), Holocene slip-rate on the Gowk strike-slip fault and implications for the distribution of tectonic strain in eastern Iran, *Geophys. J. Int.*, *181*, 221–228, doi:10.1111/j.1365-246X.2010.04538.x.

Walpersdorf, A., D. Hatzfeld, H. Nankali, F. Tavakoli, F. Nilforoushan, M. Tatar, P. Vernant, J. Chéry, and F. Masson (2006), Difference in the GPS deformation pattern of North and Central Zagros (Iran), *Geophys. J. Int.*, *167*, 1077–1088.

Wetzel, L. R., D. A. Wiens, and M. C. Kleinrock (1993), Evidence from earthquake for bookshelf faulting at large non-transform ridge offsets, *Nature*, *362*, 235–237.